HHS Public Access

Author manuscript

Biochemistry. Author manuscript; available in PMC 2016 October 14.

Published in final edited form as:

Biochemistry. 2015 March 10; 54(9): 1729–1742. doi:10.1021/bi501252z.

Effect of an Ala81His Mutation on the Met80 Loop Dynamics of Iso-1-Cytochrome *c*†

Swati Bandi‡ and **Bruce E. Bowler***

Department of Chemistry & Biochemistry, Center for Biomolecular Structure and Dynamics, University of Montana, Missoula, Montana 59812

Abstract

An A81H variant of yeast iso-1-cytochrome *c* is prepared to test the hypothesis that the steric size of the amino acid at sequence position 81 of cytochrome *c*, which has evolved from Ala in yeast to Ile in mammals, slows the dynamics of the opening of the heme crevice. The A81H mutation is used both to increase steric size and to provide a probe of the dynamics of the heme crevice through measurement of the thermodynamics and kinetics of the His81-mediated alkaline conformational transition of A81H iso-1-cytochrome *c*. Thermodynamic measurements show that the native conformer is more stable than the His81-heme alkaline conformer for A81H iso-1-cytochrome *c*. $\Delta G_u^o(H_2O)$ is about 1.9 kcal/mol for formation of the His81-heme alkaline conformer. By contrast, for K79H iso-1-cytochrome *c* the native conformer is less stable than the His79-heme alkaline conformer. $\Delta G_u^o(H_2O)$ is about −0.34 kcal/mol for formation of the His79-heme alkaline conformer. pH jump and gated electron transfer kinetics demonstrate that this stabilization of the native conformer in A81H iso-1-cytochrome *c* arises primarily from a decrease in the rate constant for formation of the His81-heme alkaline conformer, $k_{f,His81}$, relative to $k_{f,His79}$ for formation of the His79-heme alkaline conformer, which forms by a similar mechanism to that observed for the His81-heme alkaline conformer. The result is discussed in terms of the effect of global protein stability on protein dynamics and in terms of optimization of the sequence of cytochrome *c* for its role as a peroxidase in the early stages of apoptosis in higher eukaryotes.

Graphical Abstract

†This research was supported by National Science Foundation grants, CHE-0910616 and CHE-1306903 to B.E.B. The Bruker microflex MALDI-ToF mass spectrometer was purchased with Major Research Instrumentation Grant CHE-1039814 from the National Science Foundation. B.E.B. acknowledges support from CoBRE grant P20GM103546 from NIGMS.

*To whom correspondence should be addressed. Telephone: (406) 243-6114. Fax: (406) 243-4227. bruce.bowler@umontana.edu.
‡Current address: Department of Pharmaceutical Sciences, University of Colorado School of Pharmacy, Aurora, Colorado 80045

ASSOCIATED CONTENT

Supporting Information

Figures S1 to S8 which include the following data for A81H iso-1-Cyt*c*: a phylogenetic tree derived from Cyt*c* sequences with the residue at position 81 mapped onto it, plots of visible absorption spectra across a range of pH, a plot of $\epsilon_{695corr}$ versus pH at 0.5 M NaCl, plots of conformational free energies versus GdnHCl concentration, typical downward pH jump data, plots of $k_{obs,4}$, $k_{obs,5}$, A_{4u} and A_{5u}, and total amplitude versus pH from the pH jump experiments. Tables S1 to S15 summarize rate constant and amplitude data for both pH jump and gated ET experiments. This material is available free of charge via the Internet at http://pubs.acs.org.

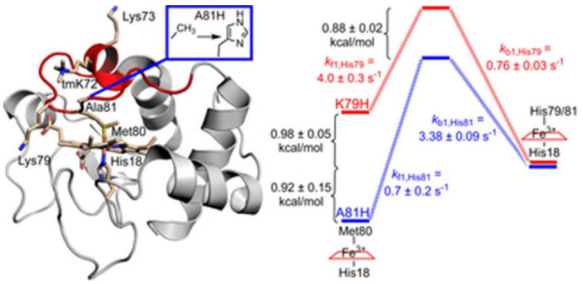

Cytochrome *c* (Cyt*c*) is a long-studied protein known to mediate electron flow between complex III and complex IV of the electron transport chain (1). Cyt*c* has also been implicated as the initiator of the caspase cascade in the intrinsic pathway of apoptosis (2, 3), through its interaction with Apaf-1 to form the apoptosome (4, 5). Recent work has shown a gain of function upon binding to cardiolipin (CL) containing membranes, with Cyt*c* acting as a peroxidase that can oxygenate the fatty acid chains of CL (6). Oxidation of CL is thought to be the earliest signal in the intrinsic pathway of apoptosis, leading to release of Cyt*c* from the intermembrane space of the mitochondria into the cytoplasm (3, 6). Loss of Met80 ligation to the heme of Cyt*c* to create an open coordination site is essential for acquisition of peroxidase activity (6–8). In the current work, we test the hypothesis that the residue at position 81 in the Ω-loop that provides the Met80 ligand to the heme (Ω-loop D (9, 10), residues 70 – 85) modulates the dynamics of Ω-loop D necessary for this function (Figure 1).

Ω-loop D has a highly conserved sequence among mitochrondrial cytochromes *c* from different species (Figure 1) (11, 12), suggesting importance for Cyt*c* function. Ω-loop D and the structurally adjacent Ω-loops B and C (residues 37 – 61) are the least stable segments of mitochondrial Cyt*c* (13–15), and thus likely to be involved in dynamics related to the function of Cyt*c*. The alkaline conformational transition of Cyt*c* (16, 17), which involves replacement of Met80 by lysines at positions 72, 73 and 79 (18–20), serves as a convenient proxy for the dynamics of Ω-loop D (21).

Studies from our lab show that mutation of Lys73 or Lys79 to histidine provides a convenient means for detailed analysis of the dynamics of the alkaline transition (17, 22–31). In contrast to earlier studies of the dynamics of the alkaline transition which have been analyzed in terms of a single ionizable trigger group (16, 32), these studies have shown that the mechanism of the alkaline transition depends on the sequence position of the ligand. When His73 provides the ligand for the alkaline state, ionization of His73 controls population of the His73-heme conformer. However, two ionizable groups with pK_a's near 5.5 and 9.0 enhance the dynamics of the alkaline transition at acidic and basic pH, respectively (23, 24, 28, 30). When His79 provides the ligand for the alkaline state, ionization of His79 is required to populate the His79-heme conformer. However, only one additional ionizable group (pK_a ~ 9) modulates the dynamics of the His79-mediated alkaline transition (26, 29, 31).

We have recently solved the structure of a K72A variant of yeast iso-1-cytochrome *c* (iso-1-Cyt*c*) with Met80 replaced by water (or hydroxide) in the 6th coordination site of the heme

(33). In this structure, the side chain of Ala81 moves to pack against Ala72. In the wild type structure, this motion would be sterically restricted by trimethyllysine 72 (tmK72), a residue that is conserved as lysine/trimethyllysine in mitochondrial Cyt*c* from over 100 species (with the exception of Cyt*c* from *tetrahymena pyriformis*, (11, 12)). The tmK72A mutation also enhances the peroxidase activity of iso-1-Cyt*c*. In higher eukaryotes, which have a fully evolved apoptotic pathway (34), position 81 is occupied by the more sterically bulky amino acid isoleucine (35) (see Figure 1B). In plants and insects, valine, a residue of intermediate steric bulk is prevalent (Figure 1B, see also Figure S1 of the Supporting Information). Based on the K72A iso-1-Cyt*c* structure (33), we hypothesized that more restrictive sterics at position 81 may have evolved to increase the stringency of activating the intrinsic pathway of apoptosis through the peroxidase activity of Cyt*c*. To test this hypothesis, we have replaced Ala81 of iso-1-Cyt*c* with a histidine (A81H variant). This mutation serves a dual function. It provides a ligand for the alkaline state that can be used to probe Ω-loop D dynamics near neutral pH and it increases the steric size of the side chain at position 81 to a size similar to isoleucine (see Figure 1B). Our thermodynamic and kinetic analysis of the A81H variant is consistent with our hypothesis that increased steric size at position 81 inhibits loss of heme-Met80 ligation. In particular, the A81H mutation appears to slow the dynamics of formation of the His81-heme alkaline conformer primarily by stabilizing of the native state (Met80-heme ligation) of iso-1-Cyt*c* with little effect on the stability of the alkaline conformer (His81-heme ligation), which appears to have similar global stability compared to other alkaline conformers with His73 or His79 as the alkaline state ligand.

EXPERIMENTAL PROCEDURES

Preparation of the A81H Variant of Yeast Iso-1-Cyt*c*

The A81H variant was prepared by the unique restriction site elimination site-directed mutagenesis method (36) using the pRS/C7.8 phagemid vector as described previously (37). Single-stranded (ss) DNA carrying the gene for wild type (WT, carries a C102S mutation to prevent disulfide dimerization during physical studies) form of the iso-1-Cyt*c* gene, *CYC1* (38), was used as template. pRS/C7.8 ssDNA was prepared from TG-1 *Escherichia coli* cells infected with the R408 helper phage (39), and phenol extraction (40) was used to remove the protein coat. The selection oligonucleotide primer *Sac*I^{-}II^{+} (37) was used to eliminate the unique *Sac*I restriction site upstream from *CYC1* and create a *Sac*II restriction site. The mutagenic oligonucleotide, d(CCCACCAAA**GTG**CATCTTGGTAC), used to affect the A81H mutation was purchased from Operon Biotechnologies, Inc. (Huntsville, Alabama). The entire coding region of *CYC1* was sequenced to confirm the mutation (Murdock DNA Sequencing Facility, University of Montana).

pRS/C7.8 phagemid DNA carrying the desired *CYC1* variant gene was transformed into the GM-3C-2 strain (41) of *Saccharomyces cerevisiae* using the LiCl method (42). Transformed cells were screened for the presence of functional iso-1-Cyt*c* using glycerol-based media plates (43). A curing procedure was used to confirm phagemid-based expression (44). The pRS/C7.8 vector was also re-isolated from transformed GM-3C-2 cells (45) and re-sequenced to confirm that no additional mutations occurred under the selective growth

conditions used to express iso-1-Cyt*c* in *S. cerevisiae*. Growth, isolation and purification of the A81H variant were done as described previously (29, 31, 46, 47).

The molecular weight of the final purified form of A81H iso-1-Cyt*c* was determined to be 12758.8 ± 1.0 g/mol (expected, 12,761.4 g/mol) using a Bruker microflex MALDI-ToF mass spectrometer calibrated with Protein Calibration Standard I (Bruker Part No. 206355) using an enhanced cubic calibration routine.

Prior to all experiments, A81H iso-1-Cyt*c* was oxidized with potassium ferricyanide (5 mg per mg of protein) and separated from oxidizing agent using a Sephadex G25 size exclusion resin equilibrated to and run with buffer appropriate to the experiment. The concentration of the protein was evaluated spectrophotometrically using absorbance at wavelengths insensitive to redox state (339, 526.5 and 542 nm) (44, 48). The degree of oxidation of was evaluated using absorbance at 550 nm (44).

GdnHCl Denaturation Monitored by CD spectroscopy

Global stability of the protein at pH 7.5 (20 mM Tris, 40 mM NaCl buffer) and 25 °C was determined by GdnHCl denaturation monitored by circular dichroism (CD) spectroscopy using an Applied Photophysics Chirascan CD spectrophotometer coupled to a Hamilton Microlab 500 titrator, as previously described (49). A 6 M guanidine hydrochloride (GdnHCl) stock solution was prepared containing, as buffer, 20 mM Tris, 40 mM NaCl, pH 7.5. The GdnHCl stock concentration was determined using refractive index measurements (50). Ellipticity was measured at 222 and 250 nm. The ellipticity at 250 nm was used as background, $\theta_{222corr} = \theta_{222} - \theta_{250}$. $\theta_{222corr}$ as a function of GdnHCl concentration was fitted to eq 1 (43) which assumes a linear free energy relationship and two-state unfolding (50, 51).

$$\theta_{222corr} = \frac{\theta_N + \left[(\theta_D + m_D[\mathrm{GdnHCl}])\exp\left\{\frac{m[\mathrm{GdnHCl}] - \Delta G^{\circ}_{u}(H_2O)}{RT}\right\}\right]}{1 + \exp\left\{\frac{m[\mathrm{GdnHCl}] - \Delta G^{\circ}_{u}(H_2O)}{RT}\right\}} \quad (1)$$

where θ_N and θ_D are the ellipticities of the native and denatured protein, respectively, at 0 M GdnHCl, m_D is the denaturant dependence of the ellipticity of the denatured state, m is the GdnHCl concentration dependence of the free energy of unfolding, ΔG_u, and $\Delta G^{o}_{u}(H_2O)$ is the free energy of unfolding extrapolated to 0 M GdnHCl. Reported parameters are the average and standard deviation of four separate titrations.

Partial Unfolding by GdnHCl Monitored at 695 nm

Partial unfolding of protein was monitored at 695 nm, A_{695}, as a function of GdnHCl concentration at pH 7.5 (20 mM Tris, 40 mM NaCl) and 22 ± 1 °C using a Beckman DU 800 spectrophotometer, as described previously (26). Briefly, equal volumes of pH 7.5 buffer and 2× protein stock (~200 μM protein in buffer) were mixed to produce a 500 μL protein sample and the GdnHCl concentration was gradually increased from 0 to 2 M as previously described (49). $A_{695corr}$ (= $A_{695} - A_{750}$) was converted to a corrected extinction coefficient, $\varepsilon_{695corr}$, using the concentration of the titration solution at 0 M GdnHCl evaluated at 570

and 580 nm using oxidized state extinction coefficients (ε_{570} = 5.2 mM^{-1} cm^{-1} and ε_{580} = 3.5 mM^{-1} cm^{-1} (48)). Plots of $\varepsilon_{695corr}$ versus GdnHCl concentration were fit to eq 2, which assumes two-state folding and a linear dependence of ΔG_u on GdnHCl concentration (50, 51).

$$\varepsilon_{695corr} = \frac{\varepsilon_N + \left[\varepsilon_D \times \exp\left\{\frac{m[GdnHCl] - \Delta G^o_u(H_2O)}{RT}\right\}\right]}{1 + \exp\left\{\frac{m[GdnHCl] - \Delta G^o_u(H_2O)}{RT}\right\}} \quad (2)$$

In eq 2, ε_N and ε_D are the corrected extinction coefficients at 695 nm of the native (Met80-ligated heme) and the denatured state, respectively. Other parameters are as in eq 1.

pH Titration Experiments

The alkaline conformational transition of A81H iso-1-Cyt*c* was monitored as a function of pH in 0.1 M NaCl with 0, 0.2, 0.3, 0.4 or 0.6 M GdnHCl. pH titrations in 0.5 M NaCl were also carried out. Titrations were carried out at 22 ± 1 °C using a Beckman DU 800 spectrophotometer, as previously described (24, 26, 28). Loss of heme-Met80 ligation was monitored at 695 nm (12). Data were corrected for instrument drift over the course of the titration using 750 nm as a baseline ($A_{695corr} = A_{695} - A_{750}$). $A_{695corr}$ was converted to the corrected extinction coefficient at 695 nm, $\varepsilon_{695corr}$, using concentration evaluated at 570 and 580 nm, as described above. Plots of $\varepsilon_{695corr}$ versus pH were fit to eq 3, which describes the equilibrium between the acid state, the native state and two alkaline conformers due to His81 and Lys73/79 outlined in Figure 3B (Results and Discussion).

$$\varepsilon_{695corr} = \varepsilon_{alk} + \frac{(\varepsilon_A - \varepsilon_{Alk}) + \left(\frac{10^{-pK_{C1}}}{1+10^{n(pK_A - pH)}}\right)(\varepsilon_N - \varepsilon_{Alk})}{1 + \left[\left(\frac{10^{-pK_{C1}}}{1+10^{n(pK_A - pH)}}\right)\left(1 + \frac{10^{-pK_{C2}}}{1+10^{(pK_a(His81) - pH)}} + \frac{10^{-pK_{C3}}}{1+10^{(pK_a(Lys73/79) - pH)}}\right)\right]} \quad (3)$$

In eq 3, ε_N is the corrected extinction coefficient at 695 nm of the Met80-heme bound native state, ε_{Alk} is the corrected extinction coefficient at 695 nm of the alkaline state, ε_A is the corrected extinction coefficient at 695 nm of the acid state. Three pH titrations were done at each GdnHCl concentration. The $\varepsilon_{695corr}$ versus pH data at 0 M GdnHCl were fit with no constraints on ε_A, ε_N and ε_{Alk}. At higher GdnHCl concentrations, the maximum value for $\varepsilon_{695corr}$ decreases. Therefore, the average value for ε_N at 0 M GdnHCl (0.61 ± 0.05 $mM^{-1}cm^{-1}$) was used as a constraint in fitting data at 0.2, 0.3, 0.4 and 0.6 M GdnHCl. The parameters pK_{C1} and pK_A are equilibrium and ionization constants, respectively, corresponding to folding from the acid state to the native state of A81H iso-1-Cyt*c*. pK_A was arbitrarily set to 5 when fitting data. pK_{C2} corresponds to the equilibrium constant for formation of the His81-heme alkaline conformer from the native state and pK_a(His81) is the ionization constant of His81. pK_{C3} corresponds to the equilibrium constant for the Lys73/79 alkaline transition and pK_a(Lys73/79) is the ionization that triggers this transition. pK_a(Lys73/79) was set to 10.8 when fitting data (18).

pH Jump Stopped-flow Experiments

All pH jump experiments were carried out at 25 °C. The starting solution for upward pH jump experiments was 20 μM protein in 0.1 M NaCl at pH 5. The starting solution for downward pH jump experiments was 20 μM protein in 0.1 M NaCl at pH 7.8. pH jump experiments were carried out by 1:1 mixing with a 20 mM buffer containing 0.1 M NaCl using an Applied Photophysics SX20 Stopped-flow Spectrometer. The final solution after mixing was 10 μM protein, 10 mM buffer, 0.1 M NaCl. Buffers used for achieving the final pH were acetic acid (pH 5 – 5.4), MES (pH 5.6 – 6.6), NaH_2PO_4 (pH 6.8 – 7.6), Tris (pH 7.8 – 8.8), H_3BO_3 (pH 9 – 10) and CAPS (pH 10 – 11.2). Buffer pH was adjusted with HCl or NaOH solutions. Data were collected on different time scales ranging from 50 to 500 s as necessary. Kinetics traces were acquired at 405 nm, the wavelength of maximum change in absorbance for the conversion between the native state and His-heme ligated alkaline state (22). Data for the upward and downward pH jump experiments were fit to triple or quadruple exponential equations (SigmaPlot, v. 7) to extract rate constants and amplitudes.

Gated Electron Transfer Experiments

Experiments were done using hexaammineruthenium(II) chloride (a_6Ru^{2+}) at pH 7.5 (10 mM phosphate buffer, 0.1 M NaCl) under anaerobic conditions using an Applied Photophysics SX20 Stopped flow Spectrometer. Hexaammineruthenium(II) chloride (a_6Ru^{2+}) was prepared by reducing commercially available $[Ru(NH_3)_6]Cl_3$ (Strem Chemicals) with zinc by the method of Fergusson and Love (52) and characterized by IR spectroscopy (53), as previously described (24, 26).

Anaerobic stopped-flow mixing of oxidized A81H iso-1-Cyt*c* with a_6Ru^{2+} was done, as described previously (28), using an Applied Photophysics SX20 Stopped-flow Spectrometer. Solutions of a_6Ru^{2+} at approximately 0.625, 1.25, 2.5, 5, 10 and 20 mM were prepared immediately before use on a dual manifold Schlenk line with argon as the inert gas. Argon-degassed buffer was cannula-transferred onto solid $[a_6Ru(II)]Cl_2$ to prepare each solution. The actual concentration of each a_6Ru^{2+} solution was determined spectophotometrically at 390 nm (ε_{390} = 35 $M^{-1}cm^{-1}$, (54)) and 400 nm (ε_{400} = 30 $M^{-1}cm^{-1}$, (55)) both before and after stopped-flow mixing. Reported concentrations are the average and standard deviation of the measurement before and after stopped-flow mixing at both wavelengths. Reduction of the heme was monitored at 550 nm. The concentration of A81H iso-1-Cyt*c* was 5 μM after mixing. Six to eight traces were collected at each a_6Ru^{2+} concentration. For all traces, 5000 points were collected logarithmically on 100 to 500 sec time scales. Analysis of the data was done using the curve fitting program, Sigma Plot (v. 7). The data were fit to triple or quadruple exponential equations.

RESULTS AND DISCUSSION

Global Unfolding by Guanidine Hydrochloride

Global stability of the A81H variant of iso-1-Cyt*c* was determined by GdnHCl denaturation monitored by CD spectroscopy. The ellipticity measured at 222 nm is plotted against GdnHCl concentration for A81H iso-1-Cyt*c* in Figure 2 (green data points). Typically, low concentrations of GdnHCl lead to curvature in the native state baseline of Cyt*c* (56). To

account for this irregularity, we use only the portion of the native state baseline after it levels out (filled symbols Figure 2) in fitting the data to eq 1 (Experimental Procedures) and assume the native state baseline is independent of GdnHCl concentration (43). The thermodynamic parameters obtained from the fits of the data to eq 1 are collected in Table 1 along with previously reported parameters for wild type (WT) iso-1-Cyt*c* (57) and variants containing K73H (58) or K79H (26) mutations in the heme crevice loop (note that WT and all variants carry a C102S mutation to prevent disulfide dimerization during physical studies). Like previously studied variants with histidine in the heme crevice loop, the A81H mutation destabilizes iso-1-Cyt*c* relative to WT iso-1-Cyt*c* and leads to a significant decrease in the denaturant *m*-value. For the K73H and K79H variants, we previously have shown that the decrease in the *m*-value results from replacement of Met80 by the engineered histidine in the heme crevice loop in advance of CD-monitored global unfolding (22, 26). In the next section, we show that the same is true for the A81H variant.

Unfolding of the Heme Crevice Loop by GdnHCl

Unfolding of the heme crevice loop by GdnHCl can be monitored through the absorbance at 695 nm. This absorbance band reports on ligation of the heme by Met80 (12). A plot of absorbance at 695 nm, $A_{695corr}$ (= $A_{695} - A_{750}$), as a function of GdnHCl concentration (Figure 2, red data points) is compared to global unfolding monitored by CD (Figure 2, green data points). It is evident that most of the Met80 ligation is lost prior to global unfolding of the A81H variant. Thus, as with the K73H and K79H variants of iso-1-Cyt*c*, global unfolding of the A81H variant occurs primarily from a partially unfolded form of the protein where Met80 is replaced by the engineered histidine in the heme crevice loop. Thermodynamic parameters from fitting the $A_{695corr}$ versus GdnHCl concentration data to eq 2 in Experimental Procedures are collected in Table 2. The $\Delta G^{o}_{u}(H_2O)$ obtained from the fit to the data is considerably more positive than that for the previously reported K73H and K79H variants (Table 2) indicating that partial unfolding mediated by His81 binding to the heme is not as favorable as that facilitated by histidines engineered at positions 73 or 79. Given that global unfolding from the His81-heme conformer and partial unfolding from the native to the His81-heme conformer are fairly well separated (Figure 2), the effect of the A81H mutation on the stability of the native state can be approximated as the sum of $\Delta G^{o}_{u}(H_2O)$ for global (Table 1) and partial (Table 2) unfolding, yielding a stability for the native state (Met80-heme ligation) of A81H iso-1-Cyt*c* of ~6.8 kcal/mol. Thus, the A81H mutation stabilizes the native state of iso-1-Cyt*c* relative to WT iso-1-Cyt*c* by ~1 kcal/mol (see Table 1). The *m*-value for His81-mediated sub-global unfolding is larger than for His73- or His79-mediated sub-global unfolding.

pH and GdnHCl Dependence of the Native Heme-Met 80 Conformer Stability

The conformational stability for the A81H variant was monitored through the acid and alkaline transitions at a series of GdnHCl concentrations (Figure 3A). Changes in the band at 695 nm characteristic of Met80-heme ligation were followed from pH 2 to 11. For comparison, data for WT iso-1-Cyt*c* at 0 M GdnHCl is provided (Figure 3A, open circles). An increase in the absorbance band at 695 nm is observed between pH 3 and 5 followed by a decrease in the alkaline region. Comparison of the 0 M GdnHCl data for WT and A81H iso-1-Cyt*c*, shows that the A81H variant has essentially fully native Met80-heme ligation

near pH 5.5. In the alkaline region two phases are evident, a more shallow loss in absorbance at 695 nm from pH 6 to 8, which we assign to replacement of Met80 by His81 and a steeper loss of absorbance due to replacement of Met80 (and His81) by lysines 73 and 79 from the heme crevice loop (Figure 3) (18). The higher pH phase of the alkaline transition of the A81H variant corresponds closely to the alkaline transition of WT iso-1-Cyt*c* (Figure 3A). Plots of spectra as a function of pH for the A81H variant, show one isosbestic point in the pH region 5.4 – 8 consistent with formation of the His81-heme conformer being a two-state process and another isosbestic point for the pH range 8.2 – 11, consistent with formation of the Lys-heme conformers being essentially a two-state process (Figure S2 of the Supporting Information). The presence of multiple sets of isosbestic points from pH 2 to 5.2 indicates that the transition from the acid state at pH 2 to maximal population of the native state near pH 5.2 is a complicated process involving at least two intermediate states (Figure S3 of the Supporting Information). The complexity of acid denaturation of cytochrome *c* has been noted previously (12, 24, 59–64).

The pH dependence of the absorbance at 695 nm is not sensitive to the complexity of the acid to native state transition. Thus, we have fit the data in Figure 3A to a simplified model which approximates the acid state to native state transition as a two state process (Figure 3B). Thermodynamic parameters obtained from fits to the scheme in Figure 3B are given in Table 3. The value of pK_a(His81) is in the range of 6 to 7, irrespective of GdnHCl concentration, consistent with the pK_a expected for histidine. The value of pK_{C1} becomes less negative (i.e. less favorable) as GdnHCl concentration is increased, indicating destabilization of the native state relative to the acid denatured state at higher GdnHCl concentration. The values of both pK_{C2} (His81 binding to heme) and pK_{C3} (Lys73/79 binding to heme) become more negative (i.e. more favorable) as GdnHCl concentration is increased, indicating that both these states are stabilized with respect to the native state at higher GdnHCl concentration. pH titration data were also collected in the presence of 0.5 M NaCl (Figure S4 of the Supporting Information). The effect of increased NaCl concentration on the thermodynamic parameters obtained for acid and alkaline unfolding is modest (Table 3), indicating that the effect of GdnHCl on the relative stabilities of the different conformers of A81H iso-1-Cyt*c* is due primarily to the denaturing property of GdnHCl and not electrostatic screening (GdnHCl is also a salt).

After converting the pK_C's in Table 3 to free energies ($\Delta G_C = ln(10)RTpK_C$), plots of ΔG_C versus GdnHCl concentration can be fit to a linear free energy relationship ($\Delta G_C = \Delta G^o_C(H_2O) - m$[GdnHCl], Figure S5 of the Supporting Information). The $\Delta G^o_{C2}(H_2O)$ of 1.6 ± 0.2 kcal/mol and the *m*-value of 2.7 ± 0.4 kcal mol^{-1}M^{-1} for the His81-heme alkaline conformational transition are similar to the parameters obtained from GdnHCl unfolding monitored at 695 nm (Figure 2 and Table 2). The data used in the linear free energy plots (0 to 0.6 M GdnHCl) is from GdnHCl concentrations where the partial unfolding to the His81-heme conformer and global unfolding to the denatured state do not overlap (Figure 2). The similarity of the thermodynamics parameters obtained for partial unfolding by these two different approaches, indicates that the small overlap of partial and global unfolding in Figure 2 has a minimal impact on $\Delta G^o_u(H_2O)$ and *m* reported in Tables 1 and 2 for the A81H variant. The *m*-value for partial unfolding to the His81-heme alkaline conformer of ~2.7 kcal mol^{-1}M^{-1} is larger than the *m*-value of 1.4 – 1.7 kcal mol^{-1}M^{-1} observed for the

His73-heme alkaline transition of iso-1-Cyt*c* variants with a K73H mutation (22, 49) and the *m*-value of 1.1 kcal $mol^{-1}M^{-1}$ for formation of the His79-heme alkaline conformer from the native state of K79H iso-1-Cyt*c* (Table 2). Denaturant *m*-values are proportional to the change in solvent-exposed surface area, ΔSASA, 1inked to a conformational change (51, 65). Thus, the extent of the structural disruption for the His81-mediated alkaline conformational transition appears to be somewhat larger than for the His73- or His79-mediated alkaline conformational transitions. $\Delta G^{o}_{C2}(H_2O)$ for the His81-heme alkaline transition (~1.6 ± 0.2 kcal/mol) is less favorable than for either the His73-heme or the His79-heme alkaline transitions (Table 2, see also refs. (22, 26, 29, 31, 49)). At pH 7.5 and 0 M GdnHCl, the maximal population of the His81-heme alkaline conformer for the A81H variant is about 5% compared to 75% for the His79-heme alkaline conformer of the K79H variant (Figure 4).

The linear free energy plot for the Lys-mediated alkaline transition (Figure S5 of the Supporting Information) yields an *m*-value of 2.1 ± 0.4 kcal $mol^{-1}M^{-1}$ (pK_{C3} in Figure 3B). This value is larger than that seen for the Lys79-heme alkaline conformational transition of K73H variants (0.8 – 1.1 kcal $mol^{-1}M^{-1}$, (22, 49)), suggesting that Lys73 is a significant contributor to the higher pH alkaline conformer of the A81H variant (see Figure 3B).

Typically, the conformational change between the native and the acid state of iso-1-Cyt*c* is a multi-proton process with the number of protons, *n*, being near 2.5 (66–68). For the A81H variant, $n \sim 1$ at all GdnHCl concentrations (Table 3). Previous work on a N52G variant of iso-1-Cyt*c* showed a loss in the cooperativity of the acid to native state transition with two clearly separable phases, the low pH phase with $n \sim 1.7$ and the high pH phase with $n \sim 1$ (59). The low apparent value of *n* for the A81H variant could also be due to mutation-induced loss of cooperativity in the acid unfolding of iso-1-Cyt*c*.

Kinetics of the Alkaline Conformational Transition of A81H Iso-1-Cyt*c*

The kinetics of the alkaline conformational transition of the A81H variant was studied by pH jump methods. The kinetics are expected to be complicated with up to three kinetic phases possible because His81, Lys73 and Lys 79 may all displace Met80 as a ligand for the 6th coordination site of the heme (Figure 3B). Data for upward pH jump experiments from an initial pH of 5 to final pH values of 7 to 8.8 are shown in Figure 5A. Two phases on ~300 ms and ~50 s time scales are clearly evident. However, the data are better fit to a triple than a double exponential equation (see Figure 5A) demonstrating that the longer time scale phase consists of two phases. Thus, the kinetic data are consistent with alkaline conformers with His81, Lys73 and Lys79 bound to the heme populating over this pH regime. The amplitudes of the ~300 ms and ~50 s time scale phases are similar up to pH 7.8. Above this pH, the total amplitude of the slower phases becomes dominant, as expected from our thermodynamic data (see Figure 4). The ~300 ms phase (phase one, rate constant, $k_{obs,1}$; amplitude, A_{1u}, Tables S1 and S2 of the Supporting Information) begins to appear at pH 6.2 growing slowly in amplitude up to pH 8.8 (Table S2 of the Supporting Information). The slower phases yield rate constants near 0.06 s^{-1} (phase two, rate constant, $k_{obs,2}$, and amplitude, A_{2u}, Tables S3 and S4 of the Supporting Information) and 0.02 s^{-1} (phase 3, rate constant, $k_{obs,3}$, and amplitude, A_{3u}, Table S5 of the Supporting Information) below pH 8.

We also carried out downward pH jump experiments from an initial pH of 7.8 (Figure S6 of the Supporting Information), where the amplitudes of all three phases in upward pH jump experiments are similar (Tables S2, S4 and S5 of the Supporting Information). Good correspondence between rate constants in downward and upward pH jump experiments at overlapping or adjacent pH values allowed straightforward assignment of the downward pH jump phases to phase one, two and three (rates constants, $k_{obs,1}$, $k_{obs,2}$, $k_{obs,3}$ and amplitudes, A_{1d}, A_{2d}, A_{3d}, respectively, in Tables S8 to S10 of the Supporting Information).

At pH 9 and above, additional phases become evident in the upward pH jump kinetic data. The data between pH 9 and 10.8 are better fit with a quadruple than a triple exponential equation (Figure 5B). An ~10 ms time scale phase is observed first (phase 4, rate constant, $k_{obs,4}$ and amplitude, A_{4u}, Table S6 of the Supporting Information). Above pH 8, the behavior of $k_{obs,1}$ is complex (Figure 6A). It decreases in magnitude until pH 10 and then increases again up to pH 11. Above pH 8, $k_{obs,2}$ for phase 2 and $k_{obs,3}$ for phase 3 both increase (Figure 7). However, the amplitude for phase 2 decreases above pH 8.8 whereas that for phase 3 continues to increase until pH 9.6. At pH 9.8, phases 1 and 2 become indistinguishable and a fifth phase on an ~50 ms timescale (rate constant, $k_{obs,5}$, and amplitude, A_{5u}, in Table S7 of the Supporting Information) begins to emerge. Above pH 9.6, we assume that phase 2 has disappeared due to the progressive decrease in its amplitude above pH 8.8 (Figure 7, inset) while the amplitude of phase 1 with which it merges at pH 9.8 increases progressively up to pH 10 (Figure 6B). As pH increases from 9.8 to 10.8, phases 4 and 5 progressively dominate the kinetics (Figure 5B, Tables S6 and S7 of the Supporting Information), as first phase 3 (Figure 7, inset) and then phase 1 (Figure 6B) disappear.

Assignment of Kinetic Phases of the Alkaline Conformational Transition of A81H Iso-1-Cyt*c*

As noted above, there are three potential ligands for the alkaline conformer of A81H iso-1-Cyt*c*, His 81, Lys73 and Lys 79. Below pH 9, three phases are observed, indicating that the kinetics of all three ligands is distinguishable. Phase one occurs on a time scale that is typical of alkaline conformers with His-heme ligation (Figure 6A) (17, 23–31, 69). The amplitude of phase one in upward pH jumps also grows in from pH 6.2 to 8 with some leveling out of the amplitude near pH 8 (Figure 6B). The amplitude behavior is consistent with what is expected for His81 based on the thermodynamics of the alkaline transition of A81H iso-1-Cyt*c* (Figures 3 to 5). On this basis we assign phase one of the pH jump kinetics to the His81-heme alkaline conformer.

Phases two and three occur on a time scale of tens of seconds below pH 8 (Figures 5 and 7) This time scale is typical of the kinetics of Lys-heme alkaline conformers in this pH regime (18, 32, 70). Studies on iso-1-Cyt*c* variants with only Lys73 or Lys 79 yield rate constants near 0.04 s^{-1} and 0.016 s^{-1} at low pH, respectively (18). Thus, we assign phase 2 to formation of the Lys73-heme alkaline conformer and phase 3 to formation of the Lys79-heme alkaline conformer. Up to pH 8.4, the amplitudes of phases two and three are similar. Above this pH, the amplitude of phase two increases up to pH 9 and then decreases up to pH 9.6, where phase two can no longer be distinguished from phase one. Phase three, due to the Lys79-heme alkaline conformer, dominates above pH 9.6 before disappearing at pH 11. The

discontinuity in the growth in the amplitude of phase three likely results from the similar time scale of all three phases between pH 9 and 9.6, which leads to larger errors bars on rate constants and amplitudes in this pH regime. Iso-1-Cyt*c* variants with only a single possible Lys as the alkaline state ligand yield a lower apparent pK_a for the Lys73-heme alkaline conformer than for the Lys79-heme alkaline conformer, consistent with the initial dominance of the Lys73-heme conformer observed in our pH jump data (18, 71). Furthermore, linearization of the alkaline transition data for iso-1-Cyt*c*, indicates that the Lys79-heme conformer becomes dominant at higher pH (72), consistent with the dominance of A_{3u} due to the Lys79-heme alkaline conformer over A_{2u} due to the Lys73-heme alkaline conformer above pH 9 (Figure 7, inset).

Fast phases on the 10 to 50 ms timescale have been reported for mammalian cytochromes *c* above pH 10 (21, 73–76). Typically, only a single phase is observed. These phases have been attributed to a transient intermediate, which has variously been assigned to Cyt*c* with a weakened heme-Met80 bond or displacement of Met80 by hydroxide (73, 75) or to a conformational change involving opening of the least stable substructure of Cyt*c* (21). In all studies on the alkaline transition, the rate constant for the fast phase initially decreases with increasing pH. In some studies the rate constant reaches a minimum and then increases (73–75) and in other studies the rate constant reaches a constant value at higher pH (21).

The A81H variant of iso-1-Cyt*c* shows two fast phases. Phase 5, which occurs on a 50 ms time scale, is typical of previously observed fast phases. After first appearing at pH 9.8, $k_{obs,5}$ initially decreases reaching a minimum at pH 10.8 and then increases at higher pH (Figure S7 of the Supporting Information). Thus, the behavior of $k_{obs,5}$ is consistent with the ionizable transient intermediate proposed in previous work (74, 75). The amplitude of this phase, A_{5u}, is initially constant with an abrupt increase from pH 10.6 to 11.2 (Figure S7 of the Supporting Information). The sigmoidal shape of the data can be fit to the Henderson-Hasselbalch equation with an apparent pK_a of 10.75 (Figure S7 of the Supporting Information). The abruptness of the increase in the amplitude is consistent with a multiproton process (number of protons, $n = 3.7 \pm 1.3$) affecting the population of this transient intermediate.

Phase 4 occurs on a 10 ms timescale. Within error its magnitude is constant from pH 9 to 10.6. It then appears to increase. There is a steady monotonic increase in A_{4u}, the amplitude of this phase. We have previously observed a phase on this time scale above pH 8 for a K72A/K73H variant of iso-1-Cyt*c* (29). The amplitude of this phase also grew in monotonically with pH. The origin of this 10 ms time scale phase is unclear.

The total amplitude of the alkaline conformational transition kinetics monitored at 405 nm (Figure S8 of the Supporting Information) mirrors the equilibrium data monitored at 695 nm (Figure 3), indicating that the kinetic measurements are capturing the complete conformational transition. As noted in the previous section, the slower phases (one, two and three) disappear and are replaced by the faster phases (four and five) at high pH (see Figure S8 of the Supporting Information). The apparent pK_a for the loss of the summed slow phases is 10.6, similar to the value obtained from the pH dependence of A_{5u}. The number of protons, *n*, linked to this loss in amplitude is 1.75. While *n* is smaller (in part due to

averaging over A_{1u} and A_{3u}) for loss of the slow phases than for the increase in A_{5u}, its magnitude is also indicative of the involvement of more than one ionizable group. In previous studies, pK_a's in this same range, led to the suggestion that ionization of tyrosines 48, 67, or 74 could modulate the fast phase observed at high pH for the kinetics of the alkaline conformational transition of iso-1-Cyt*c* (21, 74, 75). The apparent pK_a we observe for the transition from slow to fast phases and the number of protons involved is consistent with two or more of these residues being involved.

Extracting Microscopic Rate Constants with Conformationally-gated Electron Transfer

At low pH, pH jump kinetic studies can provide the microscopic rate constant, k_b, for the return of an alkaline conformer of Cyt*c* to the native state. At low pH, $k_{obs} \approx k_b$ when the alkaline conformer returns fully to the native state (32). In the current work, we are particularly interested in the effect of the A81H mutation on the dynamics of the His81-mediated alkaline transition. Unfortunately, $k_{obs,1}$, which corresponds to formation of the His81-heme alkaline conformer does not level out well at low pH (Figure 6 A). Thus, the magnitude of k_b for return to the native state from the His81-heme alkaline conformer, $k_{b,His81}$, is not well-defined by the pH jump data. Given our interest in understanding the effect of the A81H mutation on the dynamics of Ω-loop D, it is important to obtain an accurate value for $k_{b,His81}$.

To obtain $k_{b,His81}$ directly, we use conformationally-gated electron transfer (gated ET) methods (17, 25–28, 30, 31, 69). The kinetic square-scheme used to evaluate gated ET involving reduction of A81H iso-1-Cyt*c* by hexaammineruthenium(II), a_6Ru^{2+}, is shown in Figure 8. In our experience, the more favorable heme reduction potential of the native conformer compared to alkaline conformers of iso-1-Cyt*c* (18, 77) makes path B the dominant path for reduction of the alkaline conformer by a_6Ru^{2+} (25–28, 30, 69). For reduction of the His81-heme alkaline conformer by a_6Ru^{2+} via path B, the rate constant for gated ET, $k_{gET,2}$, is given by eq 4 (78–80).

$$k_{gET,2} = \frac{k_{b,His81} k_{ET}[a_6Ru^{2+}]}{k_{ET}[a_6Ru^{2+}] + k_{f,His81}} \quad (4)$$

When $k_{ET}[a_6Ru^{2+}] \gg k_{f,His81}$, the rate constant for gated ET, $k_{gET,2} \approx k_{b,His81}$, allowing direct evaluation of $k_{b,His81}$.

Gated ET data for reduction of A81H iso-1-Cyt*c* by a_6Ru^{2+} at pH 7.5, where the His81-heme conformer is maximally populated (Figure 4), are shown in Figure 9. Under these conditions, the native (Met80-heme) conformer, and three alkaline conformers, His81-heme, Lys79-heme and Lys73-heme, are expected to be present. Three phases are evident in the kinetic traces at all four concentrations of a_6Ru^{2+} shown. Better fits to the data are obtained with a four exponential equation (lower panel Figure 9), showing that the slowest phase is composed of two separable phases. Thus, all four species appear to be detectable in the gated ET data. The gated ET rate constants for the four phases, $k_{gET,1}$, $k_{gET,2}$, $k_{gET,3}$ and $k_{gET,4}$, are collected in Tables S12 to S15 of the Supporting Information.

The rate constant of the fastest phase, $k_{gET,1}$ increases linearly with increasing a_6Ru^{2+} concentration, consistent with direct bimolecular ET from a_6Ru^{2+} to the native state of A81H iso-1-Cyt*c* (Figure 9, inset). The slope of the dependence of the fast phase rate constant on a_6Ru^{2+} concentration yields $k_{ET} = 22 \pm 2\ mM^{-1}\ s^{-1}$. This k_{ET} is about half the value typically observed for reduction of iso-1-Cyt*c* by a_6Ru^{2+} (25, 27, 28, 69), suggesting that the A81H mutation disfavors binding of a_6Ru^{2+} at an optimal site for ET to the heme.

The rate constant for the ~300 ms time scale phase, $k_{gET,2}$, is independent of a_6Ru^{2+} concentration (Figure 9, inset), consistent with gated ET from an alkaline conformer with $k_{ET}[a_6Ru^{2+}] \gg k_{f,His81}$ at all a_6Ru^{2+} concentrations (Table S13 of the Supporting Information). The time scale of this phase assigns it to gated ET from the His81-heme alkaline conformer. The average rate constant for this phase across all a_6Ru^{2+} concentrations yields $k_{b,His81} = 3.38 \pm 0.09\ s^{-1}$. From pH jump experiments, $k_{obs,1}$ is approximately 4.1 $\pm$ 0.2 s^{-1} at pH 7.5 (see Table S1 of the Supporting Information). In pH jump data, $k_{obs,1} = k_{f,His81} + k_{b,His81}$. Therefore $k_{f,His81} = 0.7 \pm 0.2\ s^{-1}$ at pH 7.5. Evaluation of the equilibrium constant for formation of the His81-heme alkaline conformer from the native state, K_{C2}, from $k_{f,His81}$ and $k_{b,His81}$ ($K_{C2} = k_{f,His81}/ k_{b,His81}$), yields $K_{C2} = 0.21 \pm 0.06$, somewhat larger than $K_{C2} = 0.06 \pm 0.02$ obtained from equilibrium pH titration data (Figure 3 and Table 3). The relative amplitude of the direct ET phase due to the native conformer (~69%) of A81H iso-1-Cyt*c* and the gated ET phase for the His81-heme alkaline conformer (~20%) yield $K_{C2} = 0.29 \pm 0.01$, similar to the value obtained from the rate constants $k_{f,His81}$ and $k_{b,His81}$. The smaller value for K_{C2} from fitting the pH titration data (Figure 3) may in part be due to the simplification of the acid state/native state equilibrium used to fit the data (note that the fit at 0 M GdnHCl deviates most from the data between pH 4 and 8, the segment of the data which allows evaluation of pK_{C2}). We also carried out some gated ET experiments at 16 and 32 mM a_6Ru^{2+}. $k_{g,ET2}$ decreased to 1.7 $\pm$ 0.7 and 0.26 $\pm$ 0.09 s^{-1}, respectively, suggesting a decrease in $k_{b,His81}$ at high a_6Ru^{2+} concentrations. It is possible that a_6Ru^{2+} binds and stabilizes the His81-heme conformer at higher concentrations causing this decrease in $k_{b,His81}$.

The two slower phases from the gated ET experiments have rate constants of ~0.06 s^{-1} and ~0.02 s^{-1} at all a_6Ru^{2+} concentrations (Tables S14 and S15 of the Supporting Information), consistent with $k_{obs,2}$ and $k_{obs,3}$ at pH 7.8 from pH jump experiments. Thus, they can be assigned to the Lys73-heme and Lys79-heme alkaline conformers, respectively. Amplitude data indicate that the Lys79-heme conformer makes up ~7% and the Lys 73-heme conformer about ~4% of species in solution at pH 7.5, which is consistent with the combined population of Lys-heme alkaline conformers of ~10% at pH 7.5 (Figure 4) predicted by the thermodynamics parameters at 0 M GdnHCl in Table 3.

Mechanism of the His81-mediated Alkaline Conformational Transition of Iso-1-Cyt*c*

The kinetics of formation of the His81-heme alkaline conformer with the A81H variant is similar to the kinetics of formation of the His79-heme alkaline conform er with the K79H variant, reported on previously (26, 29). In both cases, the magnitude of the observed rate constant ($k_{obs,1}$ in Figure 6) rises initially from pH 5 to 7 decreases above pH 8 and then increases again above pH 10 (for the His79-heme alkaline conformer, see Figure 6 in ref

(26)). The maximal value of the observed rate constant is similar near pH 8 for both variants as is the minimum value near pH 10. In the case of K79H iso-1-Cyt*c*, the dominant form of the protein between pH 7 and 8 is the His79-heme alkaline conformer, whereas for A81H iso-1-Cyt*c*, the native conformer dominates in this pH regime (Figure 4). The proximity of both engineered histidines to Met80 may account for the similarities in the pH dependence of their kinetic behavior and suggests that the mechanism (Figure 10) used to analyze the kinetics of the His79-heme alkaline transition can be used for the His81-heme alkaline transition.

In this model, the alkaline transition is controlled by ionization of a heme ligand (pK_{HL}), His81 in this case. At higher pH, ionization of another group in the protein (YH^+ in Figure 10) with an ionization constant, pK_{H2}, alters the barrier to the conformational change. This model yields eq 5 for the dependence of $k_{obs,1}$ on pH.

$$k_{\mathrm{obs},1}=\left(\frac{K_{\mathrm{HL}}}{K_{\mathrm{HL}}+[\mathrm{H}^+]}\right)\left(\frac{k_{\mathrm{f1,His81}}[\mathrm{H}^+]+k_{\mathrm{f2,His81}}K_{\mathrm{H2}}}{K_{\mathrm{H2}}+[\mathrm{H}^+]}\right)+\left(\frac{k_{\mathrm{b1,His81}}[\mathrm{H}^+]+k_{\mathrm{b2,His81}}K_{\mathrm{H2}}}{K_{\mathrm{H2}}+[\mathrm{H}^+]}\right) \quad (5)$$

For simplicity in fitting the data in Figure 6A, we assume that pK_{H2} does not affect the equilibrium constant, K_{C2}, for the His81-heme alkaline transition. Based on the amplitude data in Figure 6B, this assumption is only adequate up to about pH 9. The solid curve in Figure 6A is a fit of eq 5 to the $k_{obs,1}$ versus pH data from pH 5 to 10 with $k_{b1,His81}$ set to 3.38 s^{-1} based on our gated ET data at pH 7.5. The fit is reasonable yielding $k_{f1,His81}$ = 0.83 ± 0.07 s^{-1} , pK_{HL} = 5.0 ± 0.3 and pK_{H2} = 9.1 ± 0.2. The value of pK_{HL} is somewhat low for a histidine. However, this value is no doubt affected by the large error bars and scatter in the $k_{obs,1}$ data below pH 7, making accurate determination of pK_{HL} difficult from the $k_{obs,1}$ data. The value obtained for pK_{H2} is comparable to that obtained for K79H variants of iso-1-Cyt*c* (26, 29), indicating that the same ionizable group affects the dynamics of both the His81-mediated and His79-mediated alkaline conformational transitions.

We can also estimate pK_{HL} from the amplitude data in Figure 6B. The behavior of A_{1u} is complex as a function of pH. However, the initial rise in the amplitude up to about pH 8 should be primarily controlled by pK_{HL}. The solid line in Figure 6B is a fit to eq 6,

$$\Delta\mathrm{A}_{1\mathrm{u}}=\Delta\mathrm{A}_{1\mathrm{u,max}}\left(\frac{1}{1+\left(\frac{k_{\mathrm{b1,His81}}}{k_{\mathrm{f1,His81}}}\right)\left(1+10^{(\mathrm{p}K_{\mathrm{HL}}-\mathrm{pH})}\right)}\right) \quad (6)$$

which assumes that the pH dependence of the amplitude depends on a single ionizable group with the ionization constant pK_{HL} (32). In eq 6, $A_{1u,max}$, is the maximal amplitude if the His81-heme alkaline conformer is completely formed. All other parameters are defined in Figure 10. The fit yields pK_{HL} = 7.06 ± 0.07, which is consistent with a histidine ionization. This value is similar to pK_a(His81) = 6.8 ± 0.4 obtained from our thermodynamic data at 0 M GdnHCl (Figure 3 and Table 3). Thus, the low value for pK_{HL} from the fit to the $k_{obs,1}$

versus pH in Figure 6A to eq 5, is likely an artifact of the small change in $k_{obs,1}$ between pH 5 and 8 combined with the larger uncertainty in the magnitude of $k_{obs,1}$ values with low amplitude in this pH regime.

Effect of the A81H Mutation on the Dynamics of the Opening of the Heme Crevice Loop

Our interest in evaluating the effect of the A81H mutation on the dynamics of the heme crevice stems from the observation that this sequence position evolves from Ala in yeast to the more sterically bulky residues Val and Ile in higher eukaryotes (Figure 1 and Figure S1 of the Supporting Information) (11, 12, 81). Our recent crystal structure of a K72A variant of iso-1-Cyt*c* with Met80 displaced from the heme shows that position 81 must move significantly to allow Met80 to swing out of the heme crevice and be replaced by water (or hydroxide). Here, the A81H mutation allows us to both monitor the dynamics of heme crevice opening and to determine the effect of a residue similar in steric bulk to Ile (Figure 1B) on the dynamics. The A81H and K79H variants of iso-1-Cyt*c* have a similar kinetic mechanism for heme crevice opening as probed by His79- or His81-mediated alkaline conformational transitions. We have previously analyzed the K79H variant by gated ET methods at pH 7.5 (26, 31). Thus, microscopic rate constants for heme crevice dynamics ($k_{f,His}$ and $k_{b,His}$) are available at this pH for both K79H iso-1-Cyt*c* and A81H iso-1-Cyt*c*, allowing the effect of the A81H mutation on the free energy landscape that controls heme crevice dynamics to be evaluated in detail.

The histidine-heme alkaline conformer provides a useful reference point for determining the effect of the A81H mutation on the free energy landscape of opening up the heme crevice with loss of Met80-heme ligation. In Figure 2, it is evident that global unfolding of A81H iso-1-Cyt*c* at pH 7.5 primarily reflects the stability of the His81-heme alkaline conformer, not the native state. Similarly, we have previously shown that global unfolding of K79H iso-1-Cyt*c* reflects the stability of the His79-heme alkaline conformer (26, 29, 31). From Table 1, the global stabilities of the His79-heme and His81-heme alkaline conformers are within error the same. If we make the assumption that denatured states of the A81H and K79H variants of iso-1-Cyt*c* have similar free energies, then we conclude the His81-heme and His79 heme alkaline conformers have the same free energy. Using microscopic rate constants from gated ET experiments, the native state of K79H iso-1-Cyt*c* is 0.98 ± 0.05 kcal/mol less stable than the His79-heme alkaline conformer. For A81H iso-1-Cyt*c*, the native state is 0.92 ± 0.15 kcal/mol more stable than the His81-heme alkaline conformer (Figure 11). Based on the relative magnitudes of $k_{b1,His79}$ and $k_{b,His81}$, the transition state (TS) for the conformational change decreases by 0.88 kcal/mol (using the Eyring equation $\Delta\Delta G^{\ddagger} = \Delta G^{\ddagger}_{His81\text{-}\ddagger} - \Delta G^{\ddagger}_{His79\text{-}\ddagger} = -RT\ln(k_{b,His81}/k_{b,His79})$. Despite this decrease in the free energy of the TS, the barrier for opening the heme crevice to allow formation of the His81-heme conformer is increased by ~1 kcal/mol based on the decrease in $k_{f1,His81}$ relative to $k_{f1,His79}$. Thus, the slowing of the kinetics of opening the heme crevice appears to result primarily from a stabilization of the native state by the A81H mutation. This observation of slower dynamics upon stabilization of the native state is consistent with the general belief based on studies of orthologous proteins from psychrophilic, mesophilic and thermophilic organisms that protein dynamics related to function is controlled by the global stability of the native conformer (82, 83). Further support for the correlation between global stability

and dynamics comes from our previous work on a K73H variant of iso-1-Cyt*c* with a destabilizing H26N mutation, which showed considerably faster dynamics for the interconversion between the native conformer and the His73-heme alkaline conformer (27, 28).

CONCLUSIONS

Our combined thermodynamic and kinetic analysis of the A81H variant of iso-1-Cyt*c* is consistent with a stabilization of the native (Met80-heme) conformer of iso-1-Cytc relative to a His81-heme alkaline conformer. This stabilization leads to a slowing of the heme crevice dynamics, consistent with the general belief that stabilization of a protein slows its dynamics. More specifically for the peroxidase function of Cyt*c* in the early stages of apoptosis (6), our recent structural studies on tmK72A iso-1-Cyt*c* (33), show that Ala81 moves significantly when Met80 is expelled from the heme crevice creating the open coordination site necessary for peroxidase activity. Mitochondrial Cyt*c* sequences show that the residue at position 81 evolves from Ala in yeast to Val and Ile in higher eukaryotes (Figure 1) (11, 81). The work presented here provides initial support for the hypothesis that the more sterically-bulky amino acids at position 81 observed in higher eukaryotes slow opening of the heme crevice required for loss of Met80 ligation to the heme, perhaps providing more stringent control of the peroxidase activity of Cyt*c* in apoptosis. Additional mutagenesis studies at position 81 will be necessary to more thoroughly vet this hypothesis.

Supplementary Material

Refer to Web version on PubMed Central for supplementary material.

Abbreviations

Cyt*c*	cytochrome *c*
CL	cardiolipin
tmK	trimethyllysine
CD	circular dichroism
GdnHCl	guanidine hydrochloride
$\Delta G^{o}_{u}(H_2O)$	free energy of unfolding in the absence of denaturant
m	rate of change of free energy of unfolding as a function of denaturant concentration
WT	wild type
gated ET	conformationally-gated electron transfer

REFERENCES

1. Winge DR. Sealing the mitochondrial respirasome. Mol. Cell. Biol. 2012; 32:2647–2652. [PubMed: 22586278]
2. Jiang X, Wang X. Cytochrome *c*-mediated apoptosis. Annu. Rev. Biochem. 2004; 73:87–106. [PubMed: 15189137]
3. Ow YP, Green DR, Hao Z, Mak TW. Cytochrome *c*: functions beyond respiration. Nat. Rev. Mol. Cell Biol. 2008; 9:532–542. [PubMed: 18568041]
4. Yu T, Wang X, Purring-Koch C, Wei Y, McLendon GL. A mutational epitope for cytochrome *c* binding to the apoptosis protease activation factor-1. J. Biol. Chem. 2001; 276:13034–13038. [PubMed: 11112785]
5. Olteanu A, Patel CN, Dedmon MM, Kennedy S, Linhoff MW, Minder CM, Potts PR, Deshmukh M, Pielak GJ. Stability and apoptotic activity of recombinant human cytochrome *c*. Biochem. Biophys. Res. Commun. 2003; 312:733–740. [PubMed: 14680826]
6. Kagan VE, Tyurin VA, Jiang J, Tyurina YY, Ritov VB, Amoscato AA, Osipov AN, Belikova NA, Kapralov AA, Kini V, Vlasova II, Zhao Q, Zou M, Di P, Svistunenko DA, Kurnikov IV, Borisenko GG. Cytochrome *c* acts as a cardiolipin oxygenase required for release of proapoptotic factors. Nat. Chem. Biol. 2005; 1:223–232. [PubMed: 16408039]
7. Wang Z, Matsuo T, Nagao S, Hirota S. Peroxidase activity enhancement of horse cytochrome *c* by dimerization. Org. Biomol. Chem. 2011; 9:4766–4769. [PubMed: 21625690]
8. Hanske J, Toffey JR, Morenz AM, Bonilla AJ, Schiavoni KH, Pletneva EV. Conformational properties of cardiolipin-bound cytochrome *c* . Proc. Natl. Acad. Sci. U.S.A. 2012; 109:125–130. [PubMed: 22190488]
9. Leszczynski JF, Rose GD. Loops in globular proteins: a novel category of secondary structure. Science. 1986; 234:849–855. [PubMed: 3775366]
10. Fetrow JS, Cardillo TS, Sherman F. Deletions and replacements of omega loops in yeast iso-1-cytochrome *c* . Proteins. 1989; 6:372–381. [PubMed: 2560195]
11. Banci L, Bertini I, Rosato A, Varani G. Mitochondrial cytochromes *c*: a comparative analysis. J. Biol. Inorg. Chem. 1999; 4:824–837. [PubMed: 10631615]
12. Moore, GR.; Pettigrew, GW. Cytochromes c: Evolutionary, Structural and Physicochemical Aspects. New York: Springer-Verlag; 1990.
13. Krishna MM, Lin Y, Rumbley JN, Englander SW. Cooperative omega loops in cytochrome *c*: role in folding and function. J. Mol. Biol. 2003; 331:29–36. [PubMed: 12875833]
14. Bai Y, Sosnick TR, Mayne L, Englander SW. Protein folding intermediates: native-state hydrogen exchange. Science. 1995; 269:192–197. [PubMed: 7618079]
15. Duncan MG, Williams MD, Bowler BE. Compressing the free energy range of substructure stabilities in iso-1-cytochrome *c* . Protein Sci. 2009; 18:1155–1164. [PubMed: 19472325]
16. Wilson, MT.; Greenwood, C. The alkaline transition in ferricytochrome *c*. In: Scott, RA.; Mauk, AG., editors. Cytochrome c: A Multidisciplinary Approach. Sausalito, CA: University Science Books; 1996. p. 611-634.
17. Cherney MM, Bowler BE. Protein dynamics and function: making new strides with an old warhorse, the alkaline conformational transition of cytochrome *c* . Coord. Chem. Rev. 2011; 255:664–677.
18. Rosell FI, Ferrer JC, Mauk AG. Proton-linked protein conformational switching: definition of the alkaline conformational transition of yeast iso-1-ferricytochrome *c* . J. Am. Chem. Soc. 1998; 120:11234–11245.
19. Maity H, Rumbley JN, Englander SW. Functional role of a protein foldon - an Omega-loop foldon controls the alkaline transition in ferricytochrome *c* . Proteins. 2006; 63:349–355. [PubMed: 16287119]
20. Ferrer JC, Guillemette JG, Bogumil R, Inglis SC, Smith M, Mauk AG. Identification of Lys79 as an iron ligand in one form of alkaline yeast iso-1-ferricytochrome *c* . J. Am. Chem. Soc. 1993; 115:7507–7508.

21. Hoang L, Maity H, Krishna MM, Lin Y, Englander SW. Folding units govern the cytochrome *c* alkaline transition. J. Mol. Biol. 2003; 331:37–43. [PubMed: 12875834]
22. Nelson CJ, Bowler BE. pH dependence of formation of a partially unfolded state of a Lys 73 -> His variant of iso-1-cytochrome *c*: implications for the alkaline conformational transition of cytochrome *c* . Biochemistry. 2000; 39:13584–13594. [PubMed: 11063596]
23. Martinez RE, Bowler BE. Proton-mediated dynamics of the alkaline conformational transition of yeast iso-1-cytochrome *c* . J. Am. Chem. Soc. 2004; 126:6751–6758. [PubMed: 15161303]
24. Baddam S, Bowler BE. Thermodynamics and kinetics of formation of the alkaline state of a Lys 79->Ala/Lys 73->His variant of iso-1-cytochrome *c* . Biochemistry. 2005; 44:14956–14968. [PubMed: 16274242]
25. Baddam S, Bowler BE. Conformationally gated electron transfer in iso-1-cytochrome *c*: engineering the rate of a conformational switch. J. Am. Chem. Soc. 2005; 127:9702–9703. [PubMed: 15998071]
26. Bandi S, Baddam S, Bowler BE. Alkaline conformational transition and gated electron transfer with a Lys 79 -> His variant of iso-1-cytochrome *c* . Biochemistry. 2007; 46:10643–10654. [PubMed: 17713929]
27. Bandi S, Bowler BE. Probing the bottom of a folding funnel using conformationally gated electron transfer reactions. J. Am. Chem. Soc. 2008; 130:7540–7541. [PubMed: 18494471]
28. Bandi S, Bowler BE. Probing the dynamics of a His73-heme alkaline conformer in a destabilized variant of yeast iso-1-cytochrome *c* with conformationally gated electron transfer methods. Biochemistry. 2011:10027–10040. [PubMed: 22026475]
29. Cherney MM, Junior C, Bowler BE. Mutation of trimethyllysine-72 to alanine enhances His79-heme mediated dynamics of iso-1-cytochrome *c* . Biochemistry. 2013; 52:837–846. [PubMed: 23311346]
30. Bandi S, Bowler BE. A cytochrome *c* electron transfer switch modulated by heme ligation and isomerization of a peptidyl-prolyl bond. Biopolymers (Pept Sci). 2013; 100:114–124.
31. Cherney MM, Junior CC, Bergquist BB, Bowler BE. Dynamics of the His79-heme alkaline transition of yeast iso-1-cytochrome *c* probed by conformationally gated electron transfer with Co(II)bis(terpyridine). J. Am. Chem. Soc. 2013; 135:12772–12782. [PubMed: 23899348]
32. Davis LA, Schejter A, Hess GP. Alkaline isomerization of oxidized cytochrome *c*. Equilibrium and kinetic measurements. J. Biol. Chem. 1974; 249:2624–2632. [PubMed: 4362690]
33. McClelland LJ, Mou T-C, Jeakins-Cooley ME, Sprang SR, Bowler BE. Structure of a mitochondrial cytochrome *c* conformer competent for peroxidase activity. Proc. Natl. Acad. Sci. U.S.A. 2014; 111:6648–6653. [PubMed: 24760830]
34. Laun, P.; Buettner, S.; Rinnerthaler, M.; Burhans, WC.; Breitenbach, M. Yeast Aging and Apoptosis. In: Breitenbach, M.; Jazwinski, SM.; Laun, P., editors. Subcellular Biochemistry: Aging Research in Yeast. Netherlands: Springer; 2012. p. 207-232.
35. Creighton, TE. The Biophysical Chemistry of Nucleic Acids and Proteins. Helvetian Press; 2010.
36. Deng WP, Nickoloff JA. Site-directed mutagenesis of virtually any plasmid by eliminating a unique site. Anal. Biochem. 1992; 200:81–88. [PubMed: 1595905]
37. Smith CR, Mateljevic N, Bowler BE. Effects of topology and excluded volume on protein denatured state conformational properties. Biochemistry. 2002; 41:10173–10181. [PubMed: 12146983]
38. Montgomery DL, Hall BD, Gillam S, Smith M. Identification and isolation of the yeast cytochrome *c* gene. Cell. 1978; 14:673–680. [PubMed: 210956]
39. Russel M, Kidd S, Kelley MR. An improved filamentous helper phage for generating single-stranded plasmid DNA. Gene. 1986; 45:333–338. [PubMed: 3026919]
40. Sambrook, J.; Russell, DW. Molecular Cloning: A Laboratory Manual, Third Edition. Vol. 1. Cold Spring Harbor, NY: Cold Spring Harbor Laboratory Press; 2001.
41. Faye G, Leung DW, Tatchell K, Hall BD, Smith M. Deletion mapping of sequences essential for *in vivo* transcription of the iso-1-cytochrome *c* gene. Proc. Natl. Acad. Sci. U.S.A. 1981; 78:2258–2262. [PubMed: 6264471]
42. Ito H, Fukuda Y, Murata K, Kimura A. Transformation of intact yeast cells treated with alkali cations. J. Bacteriol. 1983; 153:163–168. [PubMed: 6336730]

43. Hammack BN, Smith CR, Bowler BE. Denatured state thermodynamics: residual structure, chain stiffness and scaling factors. J. Mol. Biol. 2001; 311:1091–1104. [PubMed: 11531342]
44. Bowler BE, May K, Zaragoza T, York P, Dong A, Caughey WS. Destabilizing effects of replacing a surface lysine of cytochrome *c* with aromatic amino acids: implications for the denatured state. Biochemistry. 1993; 32:183–190. [PubMed: 8380333]
45. Strathern JN, Higgins DR. Recovery of plasmids from yeast into *Escherichia coli*: shuttle vectors. Methods Enzymol. 1991; 194:319–329. [PubMed: 2005796]
46. Redzic JS, Bowler BE. Role of hydrogen bond networks and dynamics in positive and negative cooperative stabilization of a protein. Biochemistry. 2005; 44:2900–2908. [PubMed: 15723532]
47. Wandschneider E, Hammack BN, Bowler BE. Evaluation of cooperative interactions between substructures of iso-1-cytochrome *c* using double mutant cycles. Biochemistry. 2003; 42:10659–10666. [PubMed: 12962490]
48. Margoliash E, Frohwirt N. Spectrum of horse-heart cytochrome *c* . Biochem. J. 1959; 71:570–572. [PubMed: 13638266]
49. Kristinsson R, Bowler BE. Communication of stabilizing energy between substructures of a protein. Biochemistry. 2005; 44:2349–2359. [PubMed: 15709747]
50. Pace CN. Determination and analysis of urea and guanidine hydrochloride denaturation curves. Methods Enzymol. 1986; 131:266–280. [PubMed: 3773761]
51. Schellman JA. Solvent denaturation. Biopolymers. 1978; 17:1305–1322.
52. Fergusson JE, Love JL. Ruthenium ammines. Inorganic Synthesis. 1972; 13:208–213.
53. Allen AD, Senoff CV. Preparation and infrared spectra of some ammine complexes of ruthenium (II) and ruthenium (III). Can.. J. Chem. 1967; 45:1337–1341.
54. Matsubara T, Ford PC. Photochemistry of ruthenium(II)-saturated amine complexes $Ru(NH_3)_6^{2+}$, $Ru(NH_3)_5H_2O^{2+}$, and $Ru(en)_3^{2+}$ in aqueous solution. Inorg. Chem. 1978; 17:1747–1752.
55. Meyer TJ, Taube H. Electron transfer reactions of ruthenium ammines. Inorg. Chem. 1968; 7:2369–2370.
56. Hagihara Y, Aimoto S, Fink A, Goto Y. Guanidine hydrochloride-induced folding of proteins. J. Mol. Biol. 1993; 231:180–184. [PubMed: 8389881]
57. Godbole S, Hammack B, Bowler BE. Measuring denatured state energetics: deviations from random coil behavior and implications for the folding of iso-1-cytochrome *c* . J. Mol. Biol. 2000; 296:217–228. [PubMed: 10656828]
58. Godbole S, Dong A, Garbin K, Bowler BE. A lysine 73->histidine variant of yeast iso-1-cytochrome *c*: evidence for a native-like intermediate in the unfolding pathway and implications for *m* value effects. Biochemistry. 1997; 36:119–126. [PubMed: 8993325]
59. Baddam S, Bowler BE. Mutation of asparagine 52 to glycine promotes the alkaline form of iso-1-cytochrome *c* and causes loss of cooperativity in acid unfolding. Biochemistry. 2006; 45:4611–4619. [PubMed: 16584196]
60. Stellwagen E, Babul J. Stabilization of the globular structure of ferricytochrome *c* by chloride in acidic solvents. Biochemistry. 1975; 14:5135–5140. [PubMed: 41]
61. Greenwood C, Wilson MT. Studies on ferricytochrome *c*. I. Effect of pH, ionic strength and protein denaturants on the spectra of ferricytochrome *c* . Eur. J. Biochem. 1971; 22:5–10. [PubMed: 5099216]
62. Dyson HJ, Beattie JK. Spin state and unfolding equilibria of ferricytochrome *c* in acidic solutions. J. Biol. Chem. 1982; 257:2267–2273. [PubMed: 6277891]
63. Robinson JB Jr, Strottmann JM, Stellwagen E. A globular high spin form of ferricytochrome *c* . J. Biol. Chem. 1983; 258:6772–6776. [PubMed: 6304055]
64. Drew HR, Dickerson RE. The unfolding of the cytochromes *c* in methanol and acid. J. Biol. Chem. 1978; 253:8420–8427. [PubMed: 30777]
65. Myers JK, Pace CN, Scholtz JM. Denaturant *m* values and heat capacity changes: relation to changes in accessible surface areas of protein unfolding. Protein Sci. 1995; 4:2138–2148. [PubMed: 8535251]

66. Godbole S, Bowler BE. Effect of pH on formation of a nativelike intermediate on the unfolding pathway of a Lys 73 -> His variant of yeast iso-1-cytochrome *c*. Biochemistry. 1999; 38:487–495. [PubMed: 9890932]

67. Herrmann LM, Bowler BE. Thermal denaturation of iso-1-cytochrome *c* variants: comparison with solvent denaturation. Protein Sci. 1997; 6:657–665. [PubMed: 9070448]

68. Cohen DS, Pielak GJ. Stability of yeast iso-1-cytochrome *c* as a function of pH and temperature. Protein Sci. 1994; 3:1253–1260. [PubMed: 7987220]

69. Baddam S, Bowler BE. Tuning the rate and pH accessibility of a conformational electron transfer gate. Inorg. Chem. 2006; 45:6338–6346. [PubMed: 16878944]

70. Pearce LL, Gartner AL, Smith M, Mauk AG. Mutation-induced perturbation of the cytochrome *c* alkaline transition. Biochemistry. 1989; 28:3152–3156. [PubMed: 2545249]

71. Battistuzzi G, Borsari M, De Rienzo F, Di Rocco G, Ranieri A, Sola M. Free energy of transition for the individual alkaline conformers of yeast iso-1-cytochrome *c* . Biochemistry. 2007; 46:1694–1702. [PubMed: 17243773]

72. Blouin C, Guillemette JG, Wallace CJA. Resolving the individual components of a pH induced conformational change. Biophys. J. 2001; 81:2331–2338. [PubMed: 11566802]

73. Saigo S. A transient spin-state change during alkaline isomerization of ferricytochrome *c* . J. Biochem. 1981; 89:1977–1980. [PubMed: 6270075]

74. Saigo S. Kinetic and equilibrium studies of alkaline isomerization of vertebrate cytochromes *c* . Biochim. Biophys. Acta. 1981; 669:13–20. [PubMed: 6271238]

75. Kihara H, Saigo S, Nakatani H, Hiromi K, Ikeda-Saito M, Iizuka T. Kinetic study of isomerization of ferricytochrome *c* at alkaline pH. Biochim. Biophys. Acta. 1976; 430:225–243. [PubMed: 6059]

76. Hasumi H. Kinetic studies on isomerization of ferricytochrome *c* in alkaline and acid pH ranges by the circular dichroism stopped-flow method. Biochim. Biophys. Acta. 1980; 626:265–276. [PubMed: 6260152]

77. Bortolotti CA, Paltrinieri L, Monari S, Ranieri A, Borsari M, Battistuzzi G, Sola M. A surface-immobilized cytochrome *c* variant provides a pH-controlled molecular switch. Chem Sci. 2012; 3:807–810.

78. Rorabacher DB. Electron transfer by copper centers. Chem. Rev. 2004; 104:651–697. [PubMed: 14871138]

79. Wijetunge P, Kulatilleke CP, Dressel LT, Heeg MJ, Ochrymowycz LA, Rorabacher DB. Effect of conformational constraints on gated electron-transfer kinetics. 3. Copper(II/I) complexes with cis- and trans-cyclopentanediyl-1,4,8,11-tetrathiacyclotetradecane. Inorg. Chem. 2000; 39:2897–2905. [PubMed: 11232830]

80. Meagher NE, Juntunen KL, Salhi CA, Ochrymowycz LA, Rorabacher DB. Gated electron-transfer behavior in copper(II/I) systems. Comparison of the kinetics for homogeneous cross reactions, NMR self-exchange relaxation, and electrochemical data for a copper macrocyclic tetrathioether complex in aqueous solution. J. Am. Chem. Soc. 1992; 114:10411–10420.

81. Fitch WM. The molecular evolution of cytochrome *c* in eukaryotes. J. Mol. Evol. 1976; 8:13–40. [PubMed: 181584]

82. D'Amico S, Marx JC, Gerday C, Feller G. Activity-stability relationships in extremophilic enzymes. J. Biol. Chem. 2003; 278:7891–7896. [PubMed: 12511577]

83. Feller G. Life at low temperatures: is disorder the driving force? Extremophiles. 2007; 11:211–216. [PubMed: 17160345]

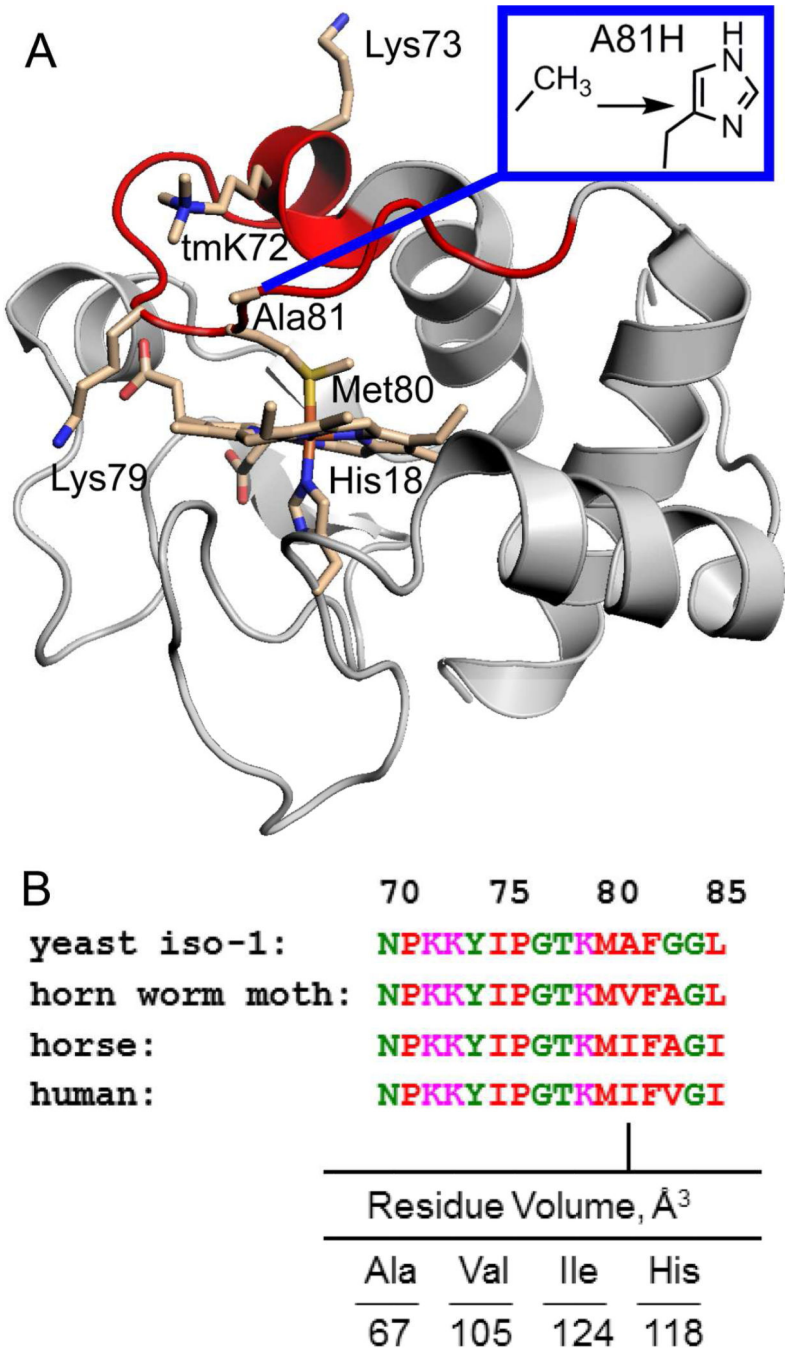

Figure 1.

(A) Iso-1-Cyt*c* shown as a gray cartoon structure with Ω-loop D (residues 70 – 85) highlighted in red. The side chains of trimethyllysine 72 (tmK72), Lys73, Lys79 and Ala81 are shown as stick models colored by element. The inset framed in blue shows the change in the side chain due to the A81H mutation. The heme cofactor and the heme ligands, Met80 and His18, are also shown colored by element. (B) Alignment of yeast iso-1-, tobacco horn worm moth, horse and human Cyt*c* sequences for the highly-conserved Ω-loop D. Residue

volumes based on van der Waals radii (35) for residues at position 81 and for histidine are provided below the alignment.

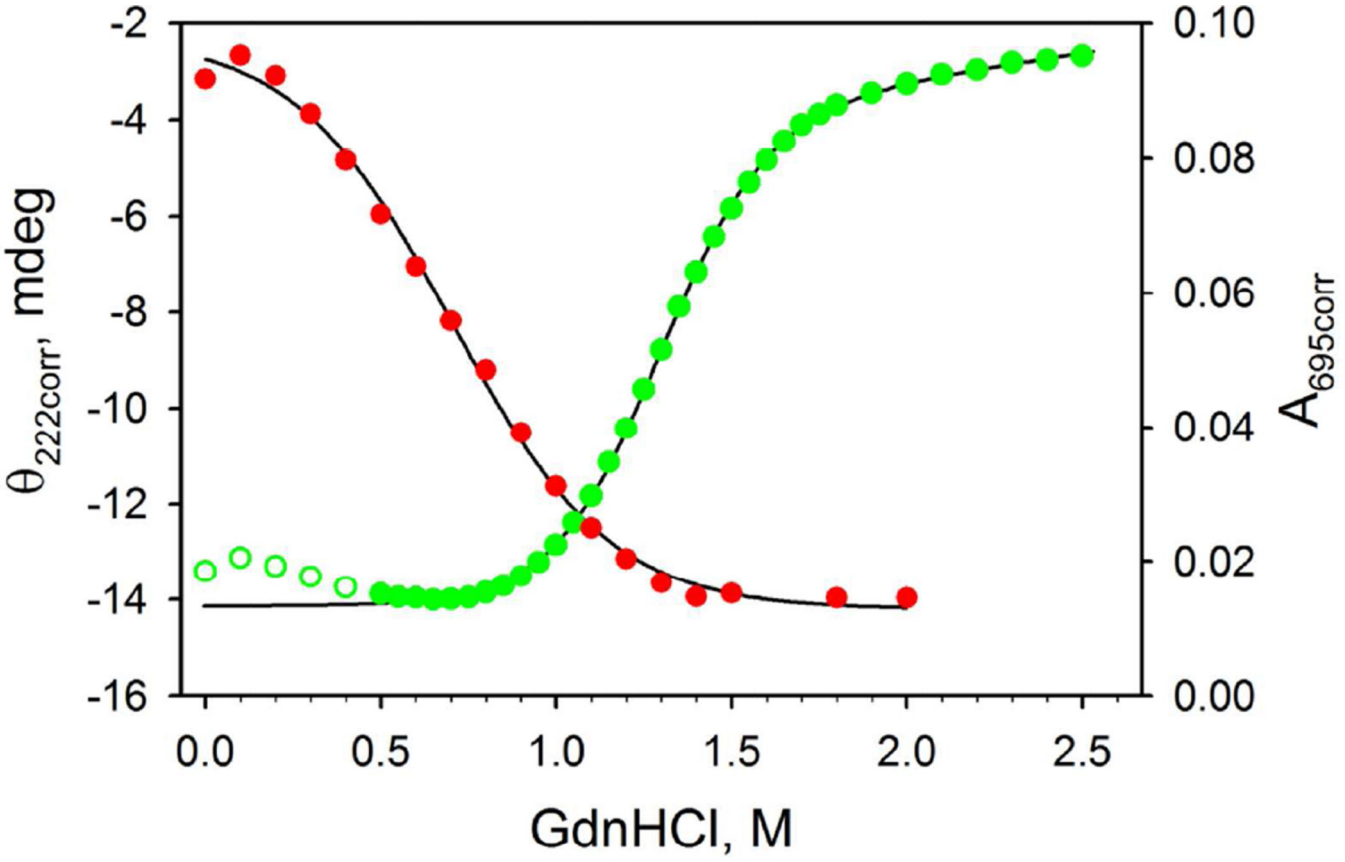

Figure 2.

GdnHCl denaturation of A81H iso-1-Cyt*c* at pH 7.5. Ellipticity at 222 nm corrected with ellipticity at 250 nm as background ($\theta_{222corr}$) is plotted as a function of GdnHCl concentration (filled and open green circles). Data were acquired at 25 °C in 20 mM Tris, pH 7.5, 40 mM NaCl and at 4 μM protein concentration. The solid curve is a fit of the data to eq 1 in Experimental Procedures using only the filled circle data. Absorbance at 695 nm corrected with absorbance at 750 nm as background ($A_{695corr}$, filled red circles) is plotted as a function of GdnHCl concentration. Data were acquired at 22 ± 1 °C in 20 mM Tris, pH 7.5, 40 mM NaCl and at ~100 μM protein concentration. The solid curve is a fit of the data to eq 2 in Experimental Procedures.

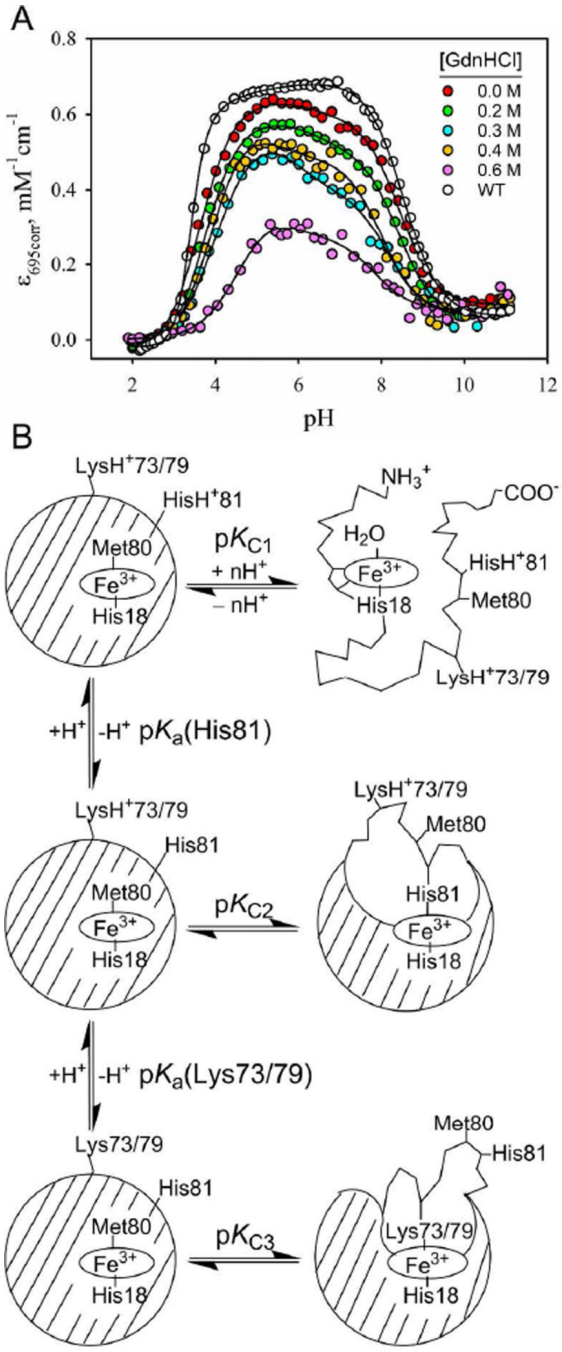

Figure 3.

(A) Plot of $\varepsilon_{695corr}$ versus pH for A81H iso-1-Cyt*c* at different concentrations of GdnHCl along with previously reported data for WT iso-1-Cyt*c* at 22 ± 1 °C in 0.1 M NaCl and 0 M GdnHCl (26). Data were collected at room temperature (22 ± 1 °C) in 0.1 M NaCl with 0, 0.2, 0.3, 0.4 and 0.6 M GdnHCl. The solid curves are fits to eq 3 as described in Experimental Procedures. (B) Equilibrium scheme used to fit the data in part A.

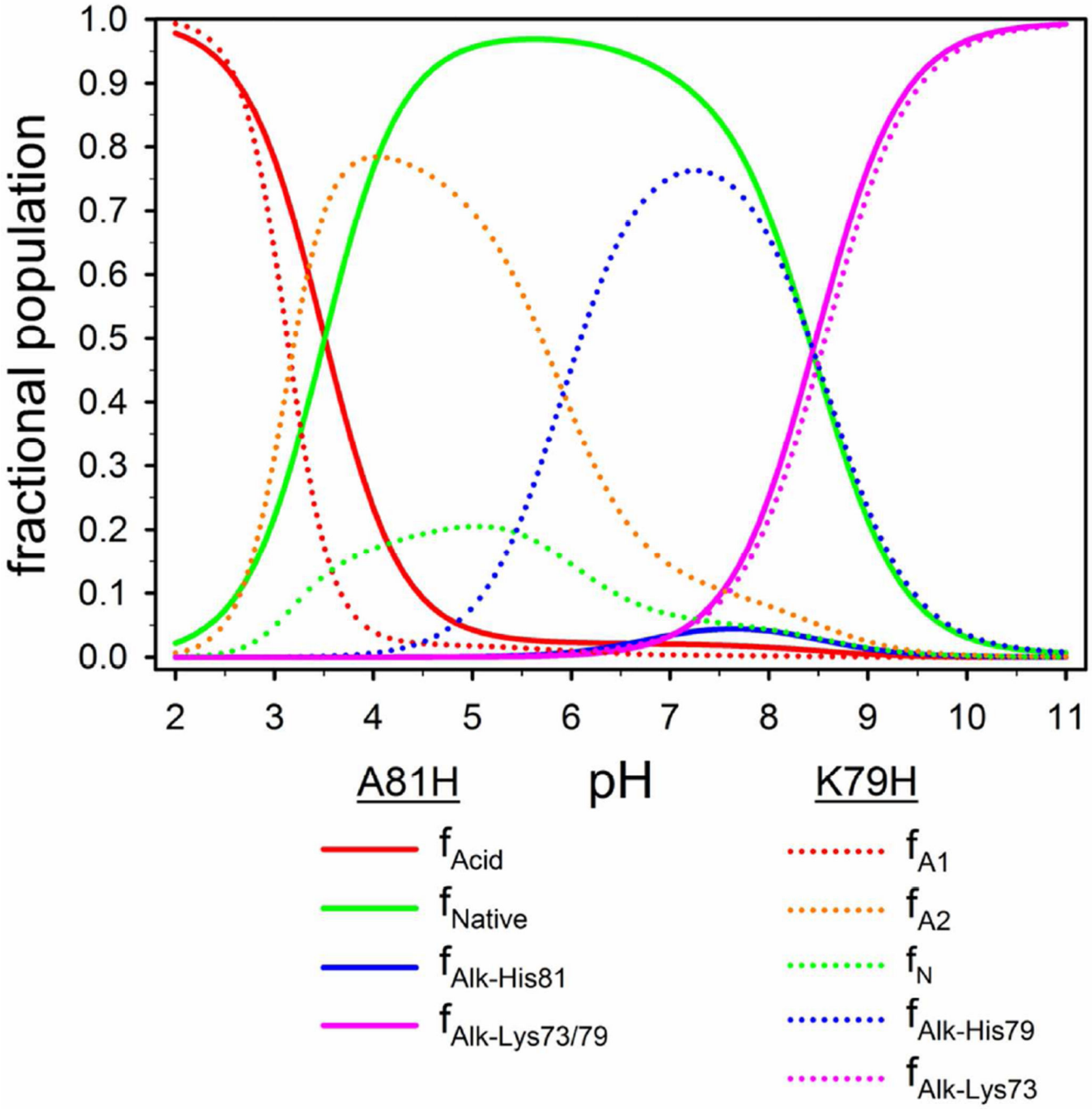

Figure 4.

Comparison of fractional population of conformers as a function of pH for A81H iso-1-Cyt*c* (solid lines) versus K79H iso-1-Cyt*c* (dashed lines). For A81H iso-1-Cyt*c*, the fractional population of the acid state, the native state, the His81-heme alkaline conformer and the Lys73/79-heme alkaline conformer are denoted by f_{Acid}, f_{Native}, $f_{Alk\text{-}His81}$ and $f_{Alk\text{-}Lys73/79}$, respectively. Fractional populations are derived from the thermodynamic parameters in Table 3 at 22 ± 1 °C in 0.1 M NaCl and 0 M GdnHCl. For K79H iso-1-Cyt*c* a thermodynamic model with two acid states was used to fit the thermodynamic data. The fractional

population of the acid 1 state, the acid 2 state, the native state, the His79-heme alkaline conformer and the Lys73-heme alkaline conformer are denoted by f_{A1}, f_{A2}, f_N, $f_{Alk\text{-}His79}$ and $f_{Alk\text{-}Lys73}$, respectively. The thermodynamics parameters used to generate the fractional populations as a function of pH are from Table 1 of ref. (26) and were obtained at 22 ± 1 °C in 0.1 M NaCl and 0 M GdnHCl.

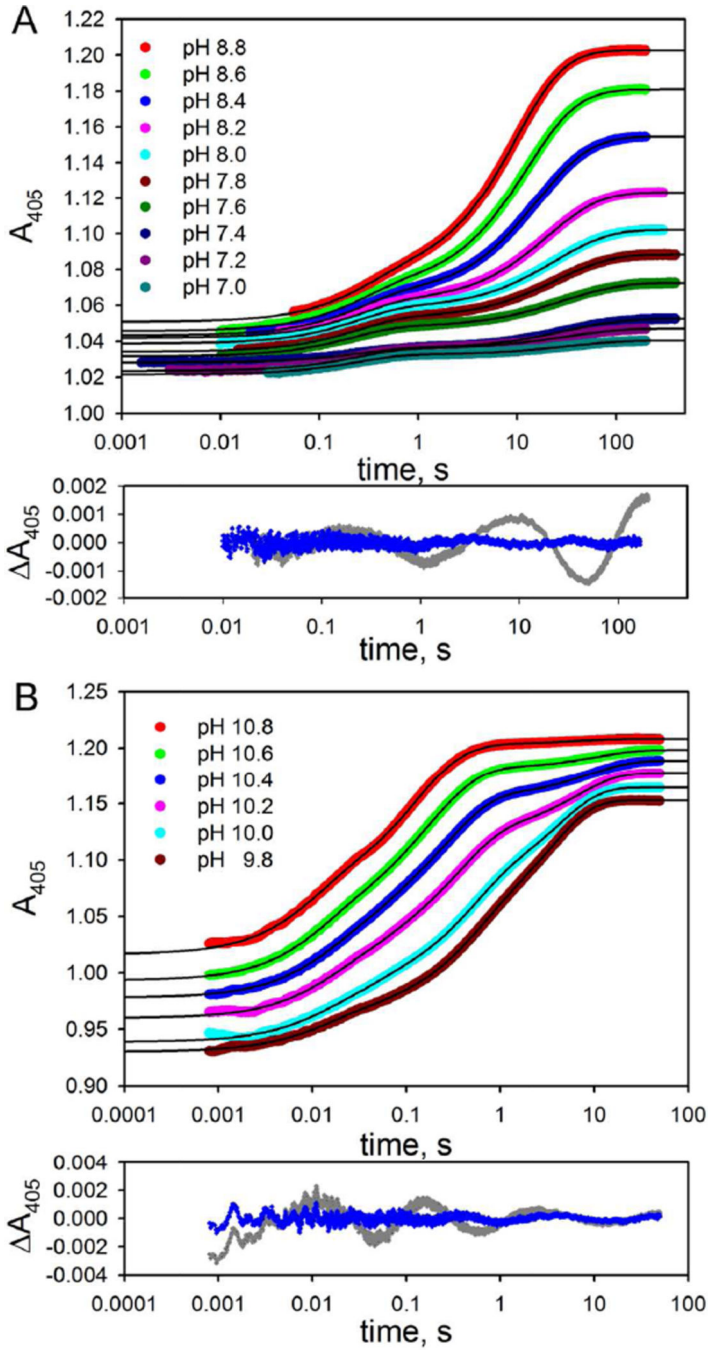

Figure 5.

Absorbance at 405 nm, A_{405}, versus time stopped-flow data for pH jump experiments from pH 5 to ending pH values of (A) 7.0 to 8.8 and (B) 9.8 to 10.8. All data were collected at 25 °C. A81H iso-1-Cyt*c* at 20 μM in 0.1 M NaCl at pH 5.0 was mixed 1:1 with a 20 mM buffer containing 0.1 M NaCl to achieve the final pH. To allow the data at different pH values to be overlaid effectively, the observed A_{405}, was adjusted at some pH values by a constant amount at every time point as follows: (A) pH 8.8 (no adjustment); pH 8.6 (A_{405} – 0.01); pH 8.4 (A_{405} – 0.01); pH 8.2 (A_{405} + 0.01); pH 8.0 (A_{405} + 0.005); pH 7.8 (A_{405}

+ 0.015); pH 7.6 (A_{405} + 0.02); pH 7.4 (A_{405} + 0.005); 7.2 (A_{405} + 0.007); 7.0 (A_{405} + 0.01) and (B) pH 10.8 (no adjustment); pH 10.6 (A_{405} – 0.015); pH 10.4 (A_{405} – 0.016); 10.2 (A_{405} – 0.045); 10.0 (A_{405} – 0.065); 9.8 (A_{405} – 0.09). The solid curves in (A) are fits to a three exponential equation. The lower panel of (A) compares residuals for the fit to a two exponential equation (gray) versus a three exponential equation (blue) at pH 8.4. The solid curves in (B) are fits to a four exponential equation. The lower panel of (B) compares residuals for the fit to a three exponential equation (gray) versus a four exponential equation (blue) at pH 10.4.

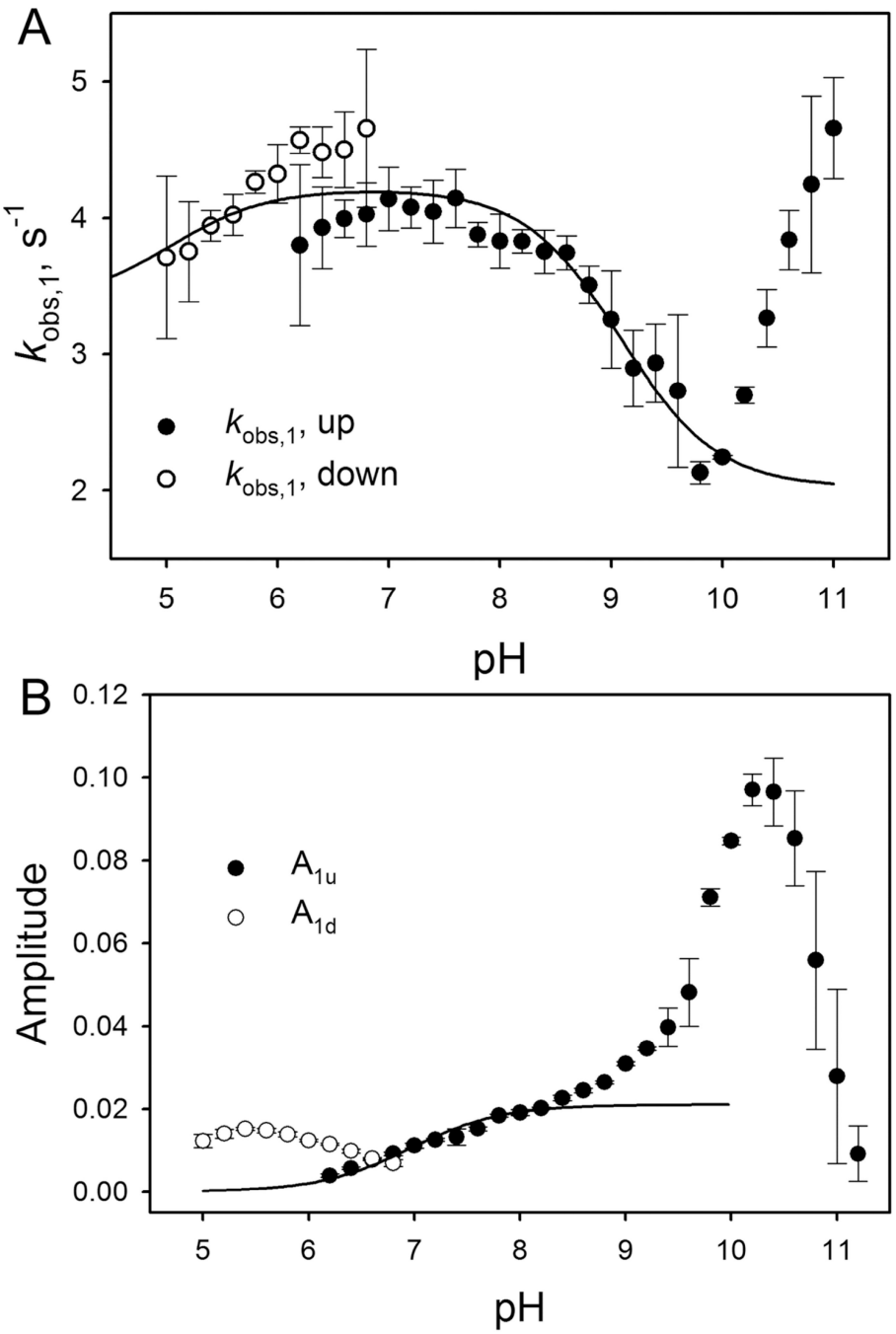

Figure 6.

(A) Plot of $k_{obs,1}$ versus pH. Data from upward pH jumps are shown with closed circles. Data from downward pH jumps are shown as open circles. (B) Plot of A_{1u} (closed circles) and A_{1d} (open circles) versus pH. Data for phase 1 were collected at 25 °C as a function of pH in 10 mM buffer containing 0.1 M NaCl. The solid curve in panel A is a fit to the kinetic model involving two ionizable groups described in the text using eq 5 (see Figure 10). The solid curve in panel B is a fit of the A_{1u} data from pH 6.2 to 8.4 to a kinetic model involving

a single ionizable group (eq 6). Rate constants and amplitudes presented in this figure are collected in Tables S1, S2 and S8 of the Supporting Information.

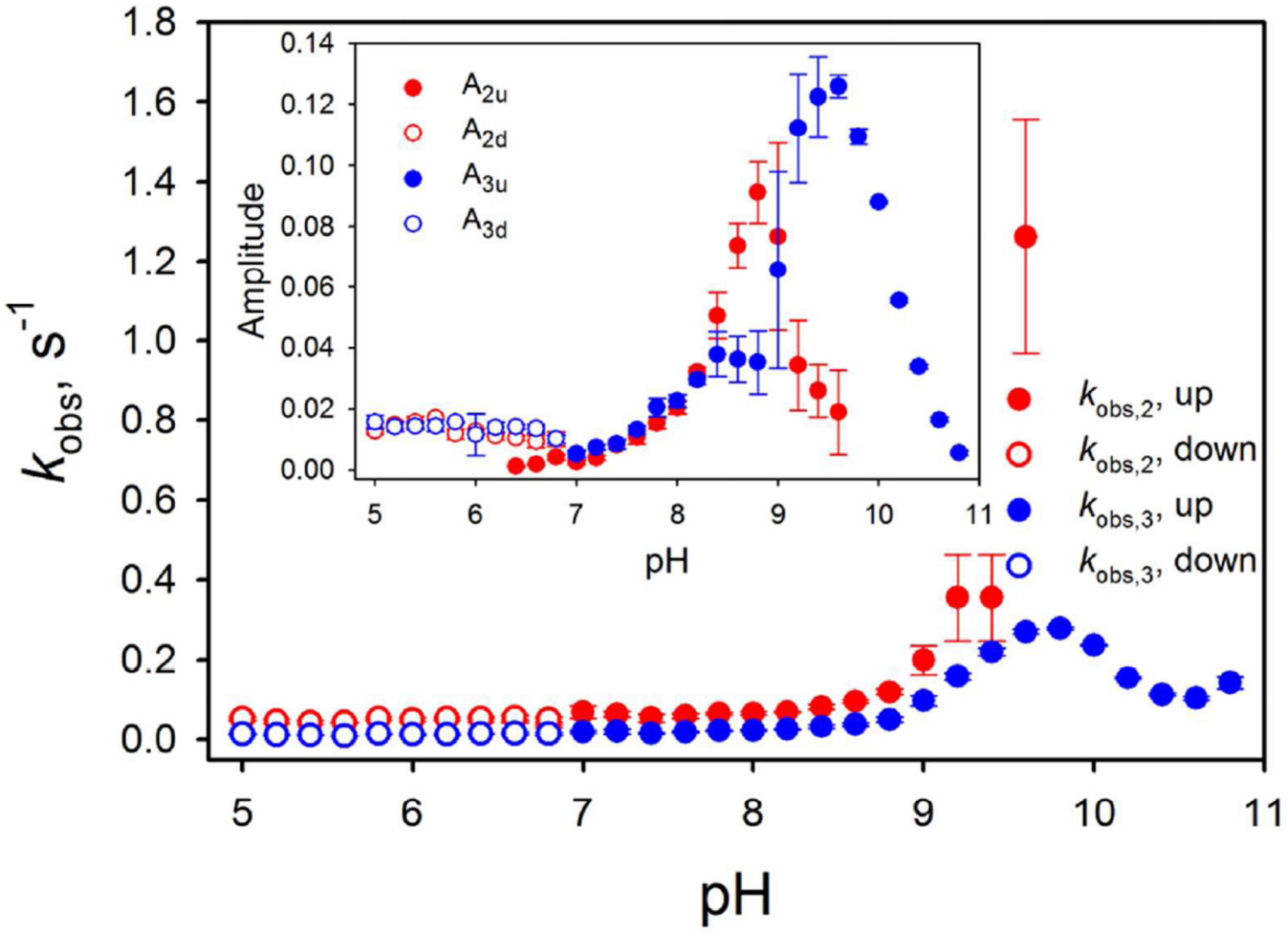

Figure 7.

Plot of rate constants for phases two and three, $k_{obs,2}$ and $k_{obs,3}$, versus pH. Data from upward pH jumps are shown with closed circles. Data from downward pH jumps are shown as open circles. The inset shows amplitude data versus pH for phases two and three. Upward pH jump amplitudes, A_{2u} and A_{3u}, are shown with closed circles. Downward pH jump amplitudes, A_{2d} and A_{3d}, are shown with open circles. Data for phase two are shown in red and for phase three in blue.

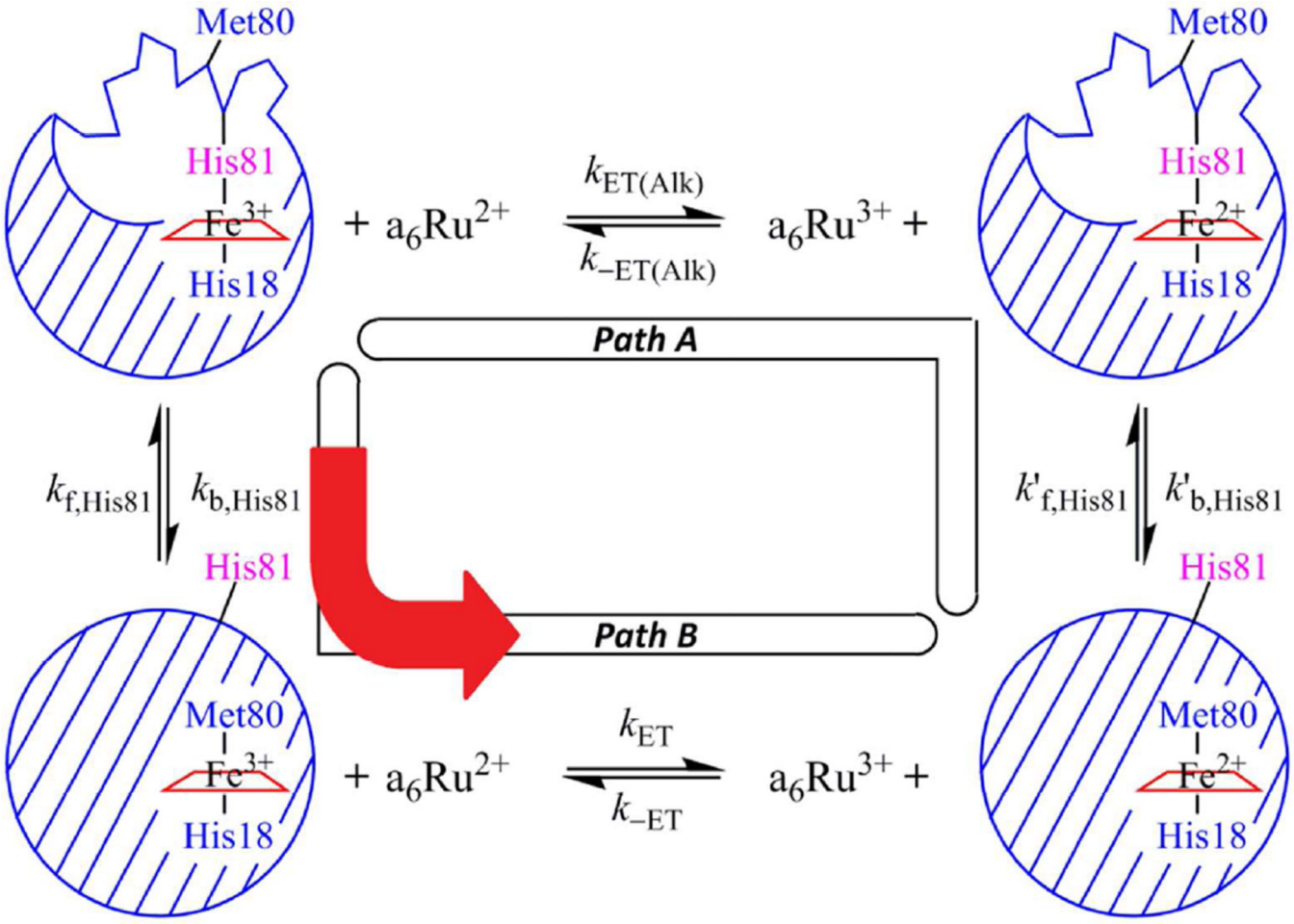

Figure 8.

Kinetic square scheme for gated ET via reduction of A81H iso-1-Cyt*c* by a_6Ru^{2+}.

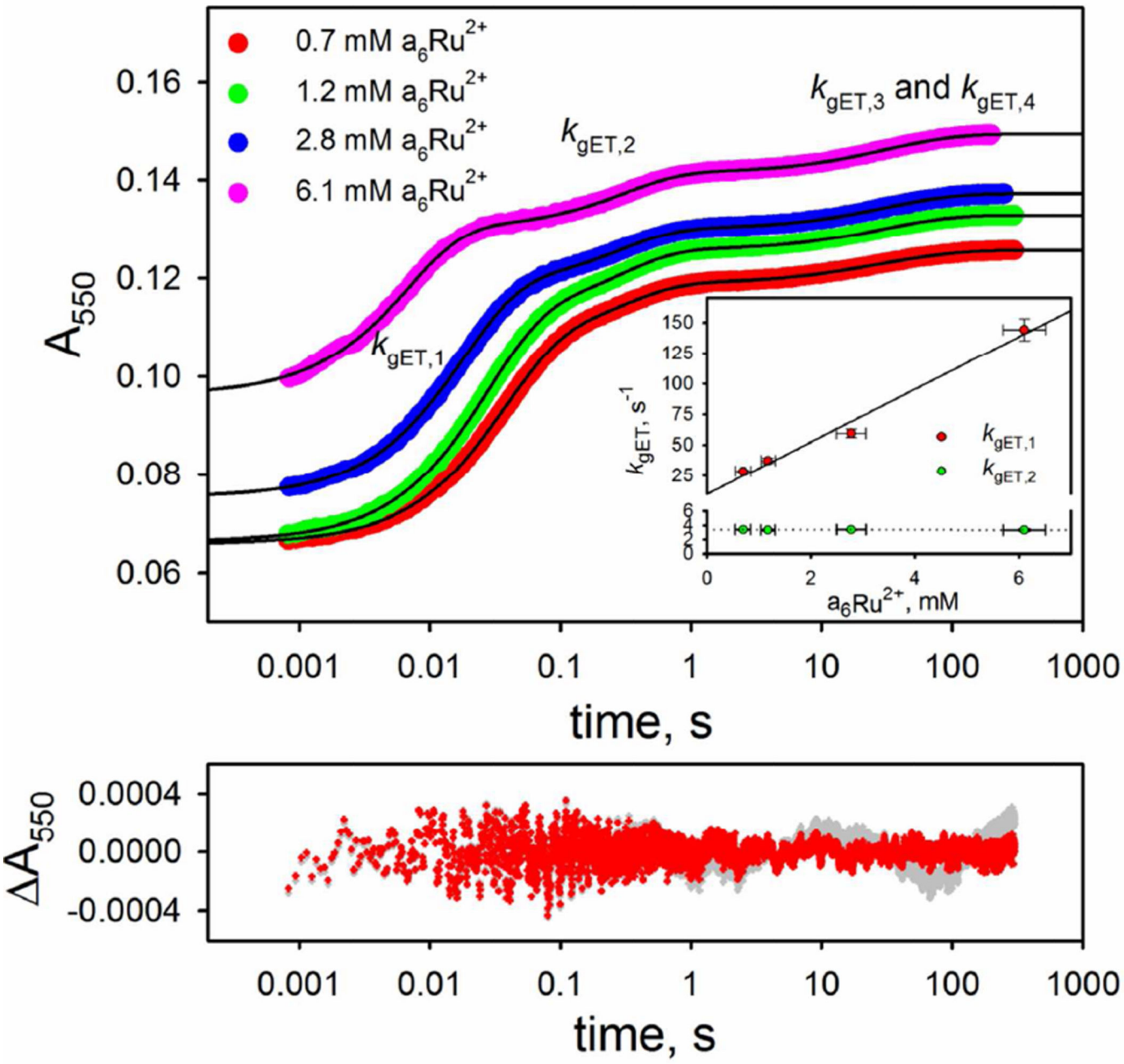

Figure 9.

Gated ET data at pH 7.5 (10 mM NaH_2PO_4, 0.1 M NaCl) and 25 °C for reduction of A81H iso-1-Cyt*c* by a_6Ru^{2+} at 0.7, 1.2, 2.8 and 6.1 mM concentrations of a_6Ru^{2+}. Solid curves are fits to a quadruple exponential equation. The inset shows plots of $k_{gET,1}$ and $k_{gET,2}$ versus a_6Ru^{2+} concentration for the reduction of the native Met80-heme conformer and the His81-heme conformer, respectively, of A81H iso-1-Cyt*c*. The lower panel compares the residuals for fits to triple (gray) exponential versus quadruple (red) exponential equations for the data acquired at 0.7 mM a_6Ru^{2+}.

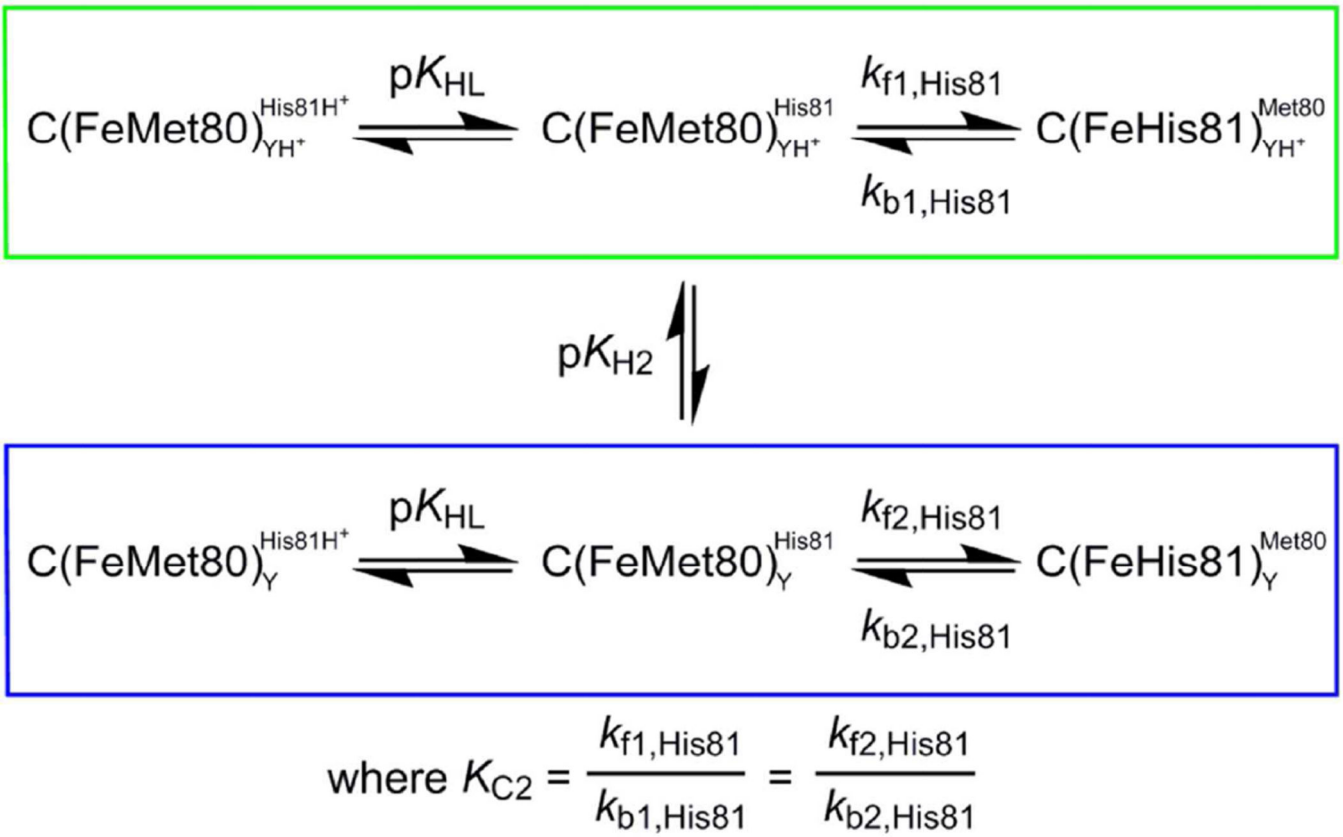

Figure 10.

Kinetic scheme involving two ionizable groups used to fit the $k_{obs,1}$ versus pH data in Figure 6A.

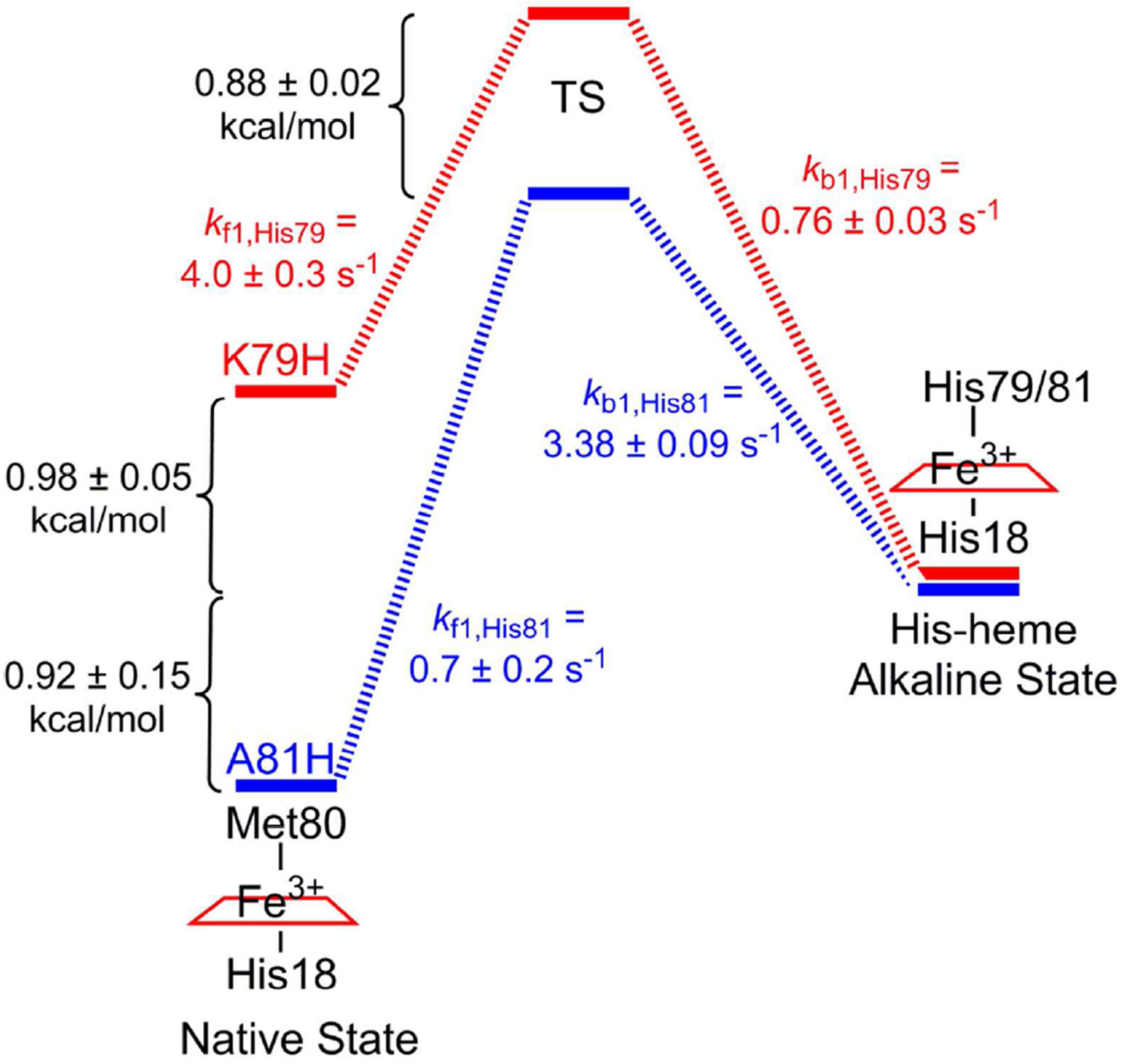

Figure 11.

Schematic representation of the effect of the A81H mutation on the relative energies of the His79/81-heme alkaline conformer, the native states of K79H and A81H iso-1-Cyt*c* and the transition state between these ground states.

Table 1

Thermodynamic Parameters for Global Unfolding of WT and Variant forms of Iso-1-Cyt*c* by GdnHCl at pH 7.5 and 25 °C.

Variant	$\Delta G_u^o(H_2O)$ (kcal/mol)	*m* (kcal/mol·M)	C_m (M)
A81H	4.89 ± 0.40	3.85 ± 0.20	1.27 ± 0.05
WT[a]	5.77 ± 0.40	5.11 ± 0.36	1.13 ± 0.02
K73H[b]	4.32 ± 0.11	3.59 ± 0.01	1.15 ± 0.01
K79H[c]	4.45 ± 0.30	3.53 ± 0.25	1.26 ± 0.01

[a]Thermodynamic parameters are from ref. (57).

[b]Thermodynamic parameters are from ref. (58).

[c]Thermodynamic parameters are from ref. (26).

Table 2

Thermodynamic Parameters for Partial Unfolding of WT and Variant forms of Iso-1-Cyt*c* by GdnHCl at pH 7.5 and 25 °C.

Variant	$\Delta G_u^o(H_2O)$ (kcal/mol)	*m* (kcal/mol·M)	C_m (M)
A81H[a]	1.87 ± 0.02	2.66 ± 0.05	0.70 ± 0.02
K73H[b]	0.38 ± 0.01	1.67 ± 0.08	0.23 ± 0.02
K79H[c]	−0.34 ± 0.11	1.0 ± 0.1	_[d]

[a]Parameters are the average and standard deviation of three trials.

[b]Thermodynamic parameters are from ref. (22).

[c]Thermodynamic parameters are from ref. (26).

[d]Fractional population of the His79-heme conformer is >0.5 at 0 M GdnHCl.

Table 3

Thermodynamic Parameters from pH Titrations in 0.1 and 0.5 M NaCl at 22 ± 1 °C for the A81H Variant of Iso-1-cytochrome *c*[a].

[GdnHCl] (M)	pK_{C1}	*n*	pK_{C2}	pK_a(His81)	pK_{C3}
0	−1.65 ± 0.20	1.11 ± 0.07	1.20 ± 0.11	6.8 ± 0.4	−2.36 ± 0.05
0[b]	−1.37 ± 0.09	0.91 ± 0.06	1.00 ± 0.14	6.7 ± 0.5	−2.34 ± 0.04
0.2	−1.49 ± 0.13	1.14 ± 0.04	0.80 ± 0.04	6.6 ± 0.1	−2.50 ± 0.04
0.3	−1.05 ± 0.10	1.04 ± 0.07	0.40 ± 0.09	6.0 ± 0.2	−2.86 ± 0.07
0.4	−1.31 ± 0.25	1.20 ± 0.19	0.55 ± 0.09	6.2 ± 0.7	−2.74 ± 0.17
0.6	−0.12 ± 0.09	0.85 ± 0.06	−0.06 ± 0.29	6.1 ± 0.9	−3.33 ± 0.14

[a]Parameters are average and standard deviation from the fits of three trials at each GdnHCl concentration to eq 3 in Experimental Procedures.

[b]Data acquired in the presence of 0.5 M NaCl.